

Highlights

- SAMP-HDRL integrates dynamic asset grouping, hierarchical agent coordination, and utility-based capital allocation to enhance portfolio robustness under non-stationary market conditions.
- Extensive backtests across three market regimes show that SAMP-HDRL outperforms nine traditional and nine DRL baselines, delivering at least 5% improvements in Return and major risk-adjusted metrics.
- SHAP-based analysis uncovers a complementary “diversified + concentrated” decision pattern across agent layers, providing transparent and interpretable insights into hierarchical DRL portfolio behavior.

SAMP-HDRL: Segmented Allocation with Momentum-Adjusted Utility for Multi-agent Portfolio Management via Hierarchical Deep Reinforcement Learning

Xiaotian Ren¹, Nuerxiati Abudurexiti², Zhengyong Jiang¹,
Angelos Stefanidis¹, Hongbin Liu^{1*}, Jionglong Su^{1*}

¹School of AI and Advanced Computing, XJTLU Entrepreneur College (Taicang), Xi'an Jiaotong-Liverpool University, Suzhou 215123, China.

²Department of Management Science and Engineering, School of Economics and Management, Xinjiang University, Urumqi 830000, China.

*Corresponding author(s). E-mail(s): Hongbin.Liu@xjtlu.edu.cn;
Jionglong.Su@xjtlu.edu.cn;

Abstract

Portfolio optimization in non-stationary markets is challenging due to regime shifts, dynamic correlations, and the limited interpretability of deep reinforcement learning (DRL) policies. We propose a Segmented Allocation with Momentum-Adjusted Utility for Multi-agent Portfolio Management via Hierarchical Deep Reinforcement Learning (SAMP-HDRL). The framework first applies dynamic asset grouping to partition the market into high-quality and ordinary subsets. An upper-level agent extracts global market signals, while lower-level agents perform intra-group allocation under mask constraints. A utility-based capital allocation mechanism integrates risky and risk-free assets, ensuring coherent coordination between global and local decisions. backtests across three market regimes (2019–2021) demonstrate that SAMP-HDRL consistently outperforms nine traditional baselines and nine DRL benchmarks under volatile and oscillating conditions. Compared with the strongest baseline, our method achieves at least 5% higher Return, 5% higher Sharpe ratio, 5% higher Sortino ratio, and 2% higher Omega ratio, with substantially larger gains observed in turbulent markets. Ablation studies confirm that upper–lower coordination, dynamic clustering, and capital allocation are indispensable to robustness. SHAP-based interpretability further reveals a complementary “diversified + concentrated”

mechanism across agents, providing transparent insights into decision-making. Overall, SAMP-HDRL embeds structural market constraints directly into the DRL pipeline, offering improved adaptability, robustness, and interpretability in complex financial environments.

Keywords: Deep Reinforcement Learning, Portfolio Management, Stock, Dynamic Clustering

1 Introduction

Portfolio management is a core component of investment strategy, aiming to maximize risk-adjusted returns while controlling exposure [Fabozzi et al. \(2008\)](#). It constitutes a foundational problem at the intersection of finance, mathematical optimization, and computational intelligence. As financial markets become increasingly volatile and data complexity increases, traditional portfolio optimization strategies encounter significant limitations in terms of modeling capacity and adaptability [Barro et al. \(2022\)](#). In recent years, Deep Reinforcement Learning (DRL) [Mnih et al. \(2015\)](#) has emerged as a powerful paradigm for portfolio management due to its ability to model sequential decision-making under uncertainty [Sutton and Barto \(1998\)](#) and to capture complex non-linear dependencies among assets [Fischer and Krauss \(2018\)](#). As an advanced framework within machine learning, DRL integrates reinforcement learning principles with deep neural architectures, thereby enabling the design of strategies that optimize long-term, risk-adjusted returns in highly volatile financial markets. DRL enables an agent to continuously interact with its environment, iteratively updating its decision-making policy to maximize long-term returns and to adaptively realize optimal investment behaviors under varying market conditions [Jiang et al. \(2024b\)](#). Benefiting from this reward-driven, self-adaptive optimization process, DRL exhibits substantial advantages in handling high-dimensional, dynamic, and nonlinear financial environments [Jiang et al. \(2024c\)](#). Compared to traditional strategies, DRL-based portfolio management not only facilitates adaptive modeling of complex market dynamics but also offers enhanced capabilities to capture nonlinear relationships, temporal dependencies, and long-term return objectives [Jiang et al. \(2024b,c\)](#), thereby establishing itself as a prominent research paradigm in intelligent investment systems.

In the domain of portfolio optimization, achieving effective allocation under dynamically evolving market conditions remains a fundamental challenge in intelligent systems research. Early studies primarily focus on holistic modeling of a single asset universe, emphasizing the use of more powerful and generalized neural architectures or advanced mathematical formulations to optimize portfolios [Jiang et al. \(2017\)](#); [Gu et al. \(2025\)](#); [Sun et al. \(2025, 2024\)](#); [Qin et al. \(2022\)](#); [Ren et al. \(2021\)](#); [Gu et al. \(2021\)](#); [Sun et al. \(2021\)](#); [Ren et al. \(2025\)](#). However, such approaches in high-dimensional spaces are highly prone to the curse of dimensionality, resulting in slow convergence, unstable training, or even divergence [Bengio et al. \(2013\)](#). To address this issue, researchers introduce clustering mechanisms to categorize assets and subsequently optimize portfolio weights through mathematical models, which subsequently

improves performance [Bulani et al. \(2025\)](#). Nevertheless, these approaches generally suffer from a fundamental limitation: the clustering and optimization processes are decoupled. Since the clustering outcomes and the optimizer cannot be jointly trained, information cannot be effectively propagated, leading to constrained policy learning or suboptimal solutions [Poli et al. \(2007\)](#). Moreover, most clustering procedures are static or rely on heuristic updates, which fail to capture the temporal dynamics of financial time series [Moody and Saffell \(2001\)](#). Consequently, when regime shifts occur in the market, such models exhibit delayed or ineffective responses, resulting in severe drawdowns, uncontrolled risk exposure, and missed opportunities for potential profit [Akgül et al. \(2025\)](#). Leveraging this, some studies attempt to integrate clustering with deep reinforcement learning, applying DRL algorithms within clustered subsets to achieve preliminary coupling between clustering and DRL [Jiang et al. \(2023\)](#); [Wang and Aste \(2023\)](#). However, clustering remains static and weakly integrated with the DRL pipeline, limiting the capacity to model dynamically changing market conditions [Yan et al. \(2024\)](#). Furthermore, certain models introduce dynamic subset selection mechanisms, restricting investment to a subset of promising assets and reducing computational complexity by maintaining a representative subset of assets through online updates [Peng et al. \(2024a\)](#); [Ma et al. \(2024\)](#). Although online updating provides promising benefits, existing mechanisms predominantly rely on heuristic rules and do not incorporate differentiable end-to-end training frameworks, thereby limiting integration with deep learning or reinforcement learning and restricting scalability as well as generalization capability [Wang and Aste \(2023\)](#). To address these issues, researchers design a two-level reinforcement learning architecture in which the upper-level agent dynamically selects stocks while the lower-level agent optimizes transaction execution, thereby alleviating to some extent the challenges posed by high-dimensional action spaces [Zhao and Welsch \(2024a\)](#). However, the stock selection process remains implicit [Zhao and Welsch \(2024a\)](#), relying entirely on the policy network's mapping from market states to actions and lacking explicit modeling of structural market shifts. Moreover, the inter-layer information flow does not constitute a genuine end-to-end feedback loop, which imposes inherent limitations on interpretability and adaptability to dynamic environments [Barto and Mahadevan \(2003a\)](#).

From a computational perspective, these approaches exhibit three major limitations.

1. Static or heuristic clustering lacks the ability to model the dynamic properties of time series. Many methods treat clustering as a one-off or low-frequency “static annotation,” [Jiang et al. \(2023\)](#); [Wang and Aste \(2023\)](#) or perform heuristic updates with fixed thresholds and simple rules, implicitly assuming that asset relationships and risk structures remain stationary within a given window [Peng et al. \(2024a\)](#); [Ma et al. \(2024\)](#). In reality, markets are highly dynamic, and such static clusters quickly become obsolete [Jiang et al. \(2023\)](#). The absence of dynamism leads to two consequences: (i) signal lag and attenuation—when regime shifts occur, outdated clusters or features lose discriminative power and strategies respond with delay [Shu et al. \(2024\)](#); and (ii) risk mismatch—risk models constrained by outdated partitions underestimate true exposures, resulting in elevated risk [Trucios \(2025\)](#). Moreover, this increases transaction costs, as misaligned rebalancing and frequent ineffective

transactions cause excessive turnover. Methodologically, it is essential to introduce risk-sensitive dynamic clustering mechanisms and deeply couple such dynamic representations with portfolio optimization in order to achieve rapid and adaptive strategy updates in evolving environments.

2. Clustering or subset selection is decoupled from the optimizer, preventing the formation of an end-to-end feedback loop. Approaches that rely on clustering or subset selection generally treat this procedure as a pre-processing stage, where the derived asset sets are subsequently passed to the optimizer or DRL module for portfolio weight learning [Bulani et al. \(2025\)](#); [Peng et al. \(2024a\)](#); [Ma et al. \(2024\)](#). The two stages neither share parameters nor provide differentiable linkages; thus, the optimizer’s objective function or DRL reward signals cannot propagate backward to influence upstream clustering or filtering strategies. This disjunction creates both objective mismatch [Trosten et al. \(2021\)](#) and distribution shift [Dulac-Arnold et al. \(2021\)](#), leading to under-utilization of information [Dulac-Arnold et al. \(2021\)](#), persistent errors [Trosten et al. \(2021\)](#), low sample efficiency [Franke et al. \(2020\)](#), slow convergence [Shi et al. \(2019\)](#), and high sensitivity to hyperparameters [Franke et al. \(2020\)](#), with the risk of becoming trapped in local optima under complex non-convex objectives [Hong et al. \(2018\)](#). Small perturbations upstream can also amplify downstream decisions, degrading stability and reproducibility [Zheng et al. \(2016\)](#). Without a closed loop, models cannot perform end-to-end uncertainty quantification and calibration, thereby weakening risk awareness and control [Kuleshov et al. \(2018\)](#). It is therefore necessary to design differentiable and feedback-aware coupling mechanisms that align asset clustering with portfolio objectives under a unified optimization paradigm.

3. Subset updating suffers from limited scalability. Rule-based dynamic subset selection cannot adaptively optimize with respect to rewards or losses [Peng et al. \(2024a\)](#); [Ma et al. \(2024\)](#), which easily introduces selection bias [Chou and Pham \(2025\)](#). The Hierarchical Reinforced Trader [Zhao and Welsch \(2024a\)](#), designed with a two-level structure of “upper-level stock selection and lower-level execution,” illustrates how hierarchical designs can partially alleviate instability and exploration difficulties in high-dimensional action spaces. Such models are generally aligned with the paradigm of hierarchical reinforcement learning (HRL) [Barto and Mahadevan \(2003b\)](#), where complex decision-making tasks are decomposed into layered subproblems to improve learning efficiency and robustness. However, the stock selection logic in these designs remains implicit, relying entirely on black-box policy networks mapping states to actions, and thus lacking explicit modeling of structural market changes [Bieganowski and Ślepaczuk \(2025\)](#). Moreover, commonly adopted alternating or staged training strategies hinder end-to-end information flow across layers, which not only exacerbates stability issues [Levy et al. \(2017\)](#) but also restricts scalability when applied to larger universes or higher-frequency trading environments. To address these challenges, it is essential to replace heuristic and black-box selection with explicit market-structure modeling, differentiable selection and allocation modules, and hierarchies that preserve informational consistency, while embedding capital allocation and risk control into a unified, utility-driven, learnable framework to enhance interpretability and scalability.

In summary, these three deficiencies collectively undermine generalization capability in real-world environments, delay responses to abrupt market transitions, and destabilize risk control. Consequently, dynamic modeling of non-stationary environments, systematic optimization around differentiable feedback loops, and scalable hierarchical architectures is not only critical for performance improvement but also a prerequisite for ensuring the practicality and reliability of knowledge-based systems in financial applications.

To address three major limitations in prevailing portfolio optimization techniques—static clustering, the lack of end-to-end integration between clustering and optimization, and reliance on heuristic subset mechanisms—we propose Segmented Allocation with momentum-adjusted utility for Multi-agent Portfolio management via Hierarchical Deep Reinforcement Learning (SAMP-HDRL), a knowledge-driven hierarchical DRL framework that integrates dynamic clustering with multi-agent decision making. In this framework, assets are dynamically partitioned into two groups through clustering. The upper-level agent operates on the complete asset universe, extracting global representations that capture inter-asset correlations and market-wide dynamics, and provides holistic guidance signals to inform subsequent decisions. The lower-level agents then focus on their respective dynamically assigned groups, allocating portfolio weights under masking constraints to ensure coherent intra-group optimization. An exponential utility function subsequently integrates the outputs of the lower-level agents with historical returns to determine segmented allocations across the two risky asset groups and the risk-free asset. On this basis, momentum adjustment and rebound detection are incorporated into the utility formulation to enhance robustness against persistent market trends and abrupt regime shifts. By design, SAMP-HDRL not only adapts to dynamic changes in market structure but also achieves a principled integration of global feature modeling, localized optimization, and risk-sensitive capital allocation. In doing so, it provides a knowledge-driven and practically scalable solution to portfolio management, directly addressing the fragmentation and rigidity observed in conventional methodologies.

This study does not introduce new neural network architectures. This study concentrates on structural innovations within the reinforcement learning framework for portfolio management. The proposed design integrates dynamic asset grouping, coordinated multi-agent allocation, and risk-sensitive utility formulation. By emphasizing structural modeling over architectural modification, the framework ensures that performance improvements originate from principled design mechanisms, thereby enhancing interpretability, robustness, and scalability in practical financial applications.

This paper has four key contributions:

1. Joint modeling of global market signals and localized asset-group decisions. Unlike conventional portfolio optimization methods that either rely on a single global model or isolate group-wise optimization, our framework first performs dynamic asset grouping, then applies an upper-level agent to extract global market representations, and finally deploys lower-level agents to allocate weights within their dynamically assigned clusters under mask constraints. This sequential design—grouping, global modeling, and local allocation—enhances representational

richness and enables more precise allocation strategies, which is empirically reflected in improved adaptability and performance stability.

2. Interpretable hierarchical decision mechanism built on dynamic classification. Leveraging dynamic asset classification, we design a hierarchical decision mechanism that eliminates the reliance on rule-based subset updating and implicit black-box selection. By explicitly modeling the grouping and allocation process within a unified learning framework, and by ensuring consistent information flow across layers, the proposed design mitigates instability caused by staged training. This approach enhances interpretability and provides stronger adaptability to structural market changes.

3. An innovative momentum-adjusted utility function for segmented allocation. We advance the utility-based allocation principle by incorporating momentum adjustment [Moskowitz et al. \(2012\)](#) and rebound detection [Jegadeesh \(1990\)](#) into the capital allocation process, which jointly accounts for historical returns, regime dynamics, and risk-free assets. This enriched utility design enhances resilience against abrupt market transitions, offering a novel mechanism for risk-sensitive and knowledge-driven portfolio optimization.

4. Consistent Outperformance in Diverse Markets SAMP-HDRL demonstrates consistent empirical performance under volatile and non-stationary market regimes. Compared with the strongest baselines, it achieves improvements of at least 5%, 5%, 5%, and 2% in Return, Sharpe Ratio, Sortino Ratio, and Omega Ratio, respectively. These results indicate that SAMP-HDRL not only enhances profitability but also delivers robust risk-adjusted performance, thereby underscoring both its theoretical contribution to reinforcement learning research and its practical significance for portfolio management.

The structure of this paper is as follows. Section 2 reviews the relevant literature and highlights recent developments in the domain of portfolio optimization and intelligent systems. Section 3 outlines the proposed methodology, covering the mathematical foundations, the design of the learning environment, and the architecture of the policy network. Section 4 presents the experimental backtests, where the performance of our framework is evaluated using portfolio value, Sharpe ratio, Sortino ratio, and Omega ratio against traditional strategies and learning-based approaches. Section 5 concludes the study and discusses possible directions for future research.

2 Related Work of Portfolio Management

In the domain of portfolio optimization, prior research primarily focuses on traditional online portfolio strategies. The Constant Rebalanced Portfolio (CRP) [Li et al. \(2023\)](#); [Kelly \(1956\)](#) and Universal Portfolios (UP) [Borodin et al. \(2000\)](#) establish the theoretical foundations of online portfolio selection by emphasizing continuous rebalancing and nonparametric universal learning, while methods such as UBAH [Cover \(1991\)](#) and the Markov of order zero (M0) model [Li and Hoi \(2014\)](#) further extend these paradigms. To capture inter-asset correlations and dynamic market characteristics, algorithms such as the Exponential Gradient (EG) [Helmbold et al. \(1998\)](#) are developed, enhancing adaptability and resilience. Alternatively, a family of mean-reversion

approaches, including Passive Aggressive Mean Reversion (PAMR) [Li et al. \(2012\)](#) and Confidence Weighted Mean Reversion (CWMR) [Li et al. \(2011b\)](#), exploits the mean-reverting tendencies of asset prices to stabilize predictive performance. Hybrid techniques that integrate nonparametric statistics with log-optimal portfolio theory, such as the Correlation-driven Nonparametric Learning Strategy (CORN) [Li et al. \(2011a\)](#), provide flexible mechanisms for leveraging structural dependencies among assets.

Beyond these algorithmic frameworks, the classical Capital Asset Pricing Model (CAPM) [Sharpe \(1964\)](#) remains a cornerstone of quantitative finance, offering a rigorous theoretical basis for asset pricing and investment allocation. Despite their foundational role, traditional strategies exhibit inherent limitations, as they are largely rule-based and struggle to adapt to complex, high-dimensional, and evolving financial environments [Xiao et al. \(2020\)](#). These constraints motivate the development of machine learning and deep reinforcement learning methods, which aim to overcome such rigidity and provide more adaptive and data-driven solutions for portfolio optimization.

In addition to these classical approaches, several alternative methodologies extend portfolio optimization beyond rule-based strategies. For example, the study on stock portfolio selection using Dempster–Shafer evidence theory [Mitra Thakur et al. \(2018\)](#) applies evidence-theoretic reasoning to quantify uncertainty and integrate heterogeneous signals, while fuzzy cross-entropy, mean, variance, and skewness models [Bhattacharyya et al. \(2014\)](#) utilize fuzzy mathematics and higher-order moments to capture non-linear risk characteristics. A hybrid two-stage robustness approach [Atta Mills and Anyomi \(2022\)](#) further formulates portfolio construction as a robust optimization problem under uncertainty, explicitly emphasizing resilience against model misspecification and market shocks. Beyond portfolio allocation, hybrid predictive models such as the efficient hybrid approach for forecasting real-time stock market indices [Kalra et al. \(2024\)](#) and the MMGAN-HPA algorithm for stock price prediction [Polamuri et al. \(2022\)](#) leverage deep generative models and multi-model integration to improve the forecasting accuracy of asset prices. While these methods enrich the methodological landscape of financial modeling, they remain primarily optimization- or prediction-driven, with limited adaptability to high-dimensional and non-stationary portfolio management environments [Chou and Pham \(2025\)](#).

Building on these developments, reinforcement learning (RL) becomes increasingly prominent in portfolio management, with research primarily emphasizing uncertainty modeling, transfer learning, expert priors, neural architecture design, and multi-objective learning, rather than asset structuring or hierarchical decision-making. Kang et al. propose the Neural Process Continuous Reinforcement Learning (NPCRL) [Kang et al. \(2024\)](#), which integrates Neural Processes with continuous-action RL to capture market uncertainty and enable dynamic rebalancing in highly volatile environments, achieving a favorable trade-off between return and risk. Representation Transfer Reinforcement Learning (RTRL) [Jiang et al. \(2024a\)](#) addresses limited samples and non-stationarity by migrating features across domains, although its benefits mainly derive from transferability rather than explicit modeling of asset structures. Choi

and Kim [Choi and Kim \(2024\)](#) design an expert-infused DRL framework that incorporates tutor policies as priors to guide dynamic allocation, demonstrating that RL agents can outperform expert strategies but focusing on knowledge infusion rather than structural modeling. An early contribution by Yang [Yang \(2023\)](#) demonstrates the feasibility of end-to-end deep RL for finance by mapping price sequences directly to portfolio weights with Convolutional Neural Networks (CNNs) [Hochreiter and Schmidhuber \(1997\)](#) and Long Short-Term Memory networks (LSTMs) [LeCun et al. \(1998\)](#), yet it does not incorporate classification, clustering, or hierarchical structures. Recent advances explore more expressive architectures: DRL-UTrans [Yang et al. \(2023\)](#) combines Transformers and U-Net to capture long-range dependencies and multi-scale patterns in financial time series, while Deep Long Short-Term Memory Q-Learning (DLQL) and its attention-based variant DLAQL [Oyewola et al. \(2024\)](#) integrate LSTMs and attention within a Q-learning framework for applications in the oil and gas sector. Other research extends RL to multi-objective optimization, such as the framework in [Xu et al. \(2023\)](#), which balances return maximization and risk control through reward design, broadening optimization objectives without modeling hierarchical or structural dependencies. Collectively, these studies provide diverse perspectives on portfolio management, yet they share common limitations [Yang \(2023\)](#); [Jiang et al. \(2023\)](#); [Fischer and Krauss \(2018\)](#): insufficient treatment of structural relationships among assets, the absence of explicit classification or clustering mechanisms, and limited adaptability and interpretability in complex and volatile financial environments [Ulm et al. \(2020\)](#). These gaps highlight the need for structural innovations that move beyond network design alone and motivate the hierarchical and clustering-based approach developed in this study.

Beyond conventional portfolio optimization and generic reinforcement learning approaches, a number of studies are more directly aligned with this work. These contributions incorporate asset structuring into portfolio management through mechanisms such as dynamic subset selection, clustering, ranking, or hierarchical organization, thereby following the paradigm of structuring assets prior to portfolio decision-making. For clarity, these studies are organized into three categories, their respective limitations are examined, and the ways in which the proposed model addresses these shortcomings are demonstrated.

In the category of clustering- or subset-based reinforcement learning methods, Dynamic Coreset Construction [Peng et al. \(2024b\)](#) dynamically constructs representative subsets to approximate the overall market distribution, thereby improving the efficiency of online portfolio selection. This mechanism can be regarded as a special form of dynamic clustering. The framework combining K-means [Jin and Han \(2010\)](#), mean-variance optimization, and reinforcement learning [Zouaghia et al. \(2025\)](#) explicitly embodies the idea of “classification followed by decision.” The CAD framework [Jiang et al. \(2023\)](#) further extracts asset correlations via clustering and integrates them with deep reinforcement learning for multi-period portfolio management. In a related direction, the clustering-based return prediction model with PSO-CNN+MVF [Ashrafpour et al. \(2023\)](#) employs clustering for stock pre-selection, followed by deep return prediction and mean-variance forecasting, thereby reducing noise and enhancing the reliability of portfolio construction. These studies collectively

Table 1 Comparison of closely related studies with our proposed model

Study	Innovation	Limitation	Our Advantage
Dynamic Coreset Construction Peng et al. (2024b)	Constructs representative subsets to approximate market distribution, improving online portfolio efficiency.	Emphasizes sampling efficiency but ignores explicit asset correlations.	Integrates dynamic clustering into RL with explicit cross-asset modeling.
Clustering + Mean-Variance + RL Zouaghia et al. (2025)	Combines clustering, mean-variance optimization, and RL to reflect a “classification then decision” paradigm.	Relies on static clusters and restrictive mean-variance assumptions.	Employs adaptive clustering and hierarchical agents, avoiding rigid constraints.
CAD: Clustering + Deep RL Jiang et al. (2023)	Incorporates clustering with deep RL for multi-period portfolio management.	Treats clustering as pre-processing with no dynamic RL interaction.	Embeds clustering directly in the RL loop with hierarchical modeling.
Clustering-based PSO-CNN+MVF Ashrafi et al. (2023)	Integrates clustering with PSO-CNN return prediction and MVF-based allocation.	Static clustering and modular design; lacks RL-driven adaptability.	Dynamic clustering within hierarchical RL ensures adaptive structuring.
Stock Ranking and Matching RL Alzaman (2025)	Uses ranking and matching signals to group assets for RL-based allocation.	Heavily depends on external signals with weak structure modeling.	Direct clustering enables adaptive and interpretable asset grouping.
ASA: Autonomous Stock Selection and Allocation Zhao and Welsch (2024b)	Applies graph/hypergraph ranking for selection and regression for allocation.	Follows a supervised paradigm with simplified risk handling.	Dynamic clustering within RL allows interactive adaptation to shifts.
HRT: Hierarchical Reinforced Trader Kim et al. (2022)	Designs a two-level hierarchy with selection at the top and execution at the bottom.	Focuses on task partitioning rather than structural asset modeling.	Our hierarchy captures both classification and cross-asset relationships.

contribute by enhancing portfolio decisions with clustering or grouping mechanisms. However, their clustering processes are mostly static, lacking dynamic interaction with reinforcement learning, which limits adaptability under non-stationary markets. In contrast, our hierarchical multi-agent framework embeds dynamic clustering directly into the training process and assigns distinct roles to lower- and upper-level agents to capture temporal dependencies and cross-asset relationships, thereby achieving stronger adaptability and structural modeling capability.

In the category of ranking- or matching-based reinforcement learning methods, the Stock Ranking and Matching RL approach [Alzaman \(2025\)](#) implicitly forms asset groups through ranking and matching mechanisms, and then optimizes portfolio selection via reinforcement learning. The ASA framework [Zhao and Welsch \(2024b\)](#) employs graph and hypergraph ranking models for stock selection, combined with classification and regression models for weight allocation. This covers the entire process from selection to allocation. These methods share the contribution of introducing

ranking or graph structures into portfolio management. Their limitations, however, lie in their reliance on external ranking signals or supervised learning paradigms, which reduces their dynamic adaptability and interactive learning capability, while risk constraints and transaction costs are simplified. In contrast, our method avoids reliance on external signals, directly models asset correlations via dynamic clustering, and achieves interactive and adaptive optimization within a reinforcement learning framework, making it better suited to non-stationary market conditions.

In the category of hierarchical structures, the Hierarchical Reinforced Trader (HRT) [Kim et al. \(2022\)](#) proposes an explicit two-level framework, where the upper level selects assets and the lower level executes transactions, thus introducing hierarchical mechanisms into portfolio management. Its contribution lies in expanding the decision structure of traditional RL. However, its hierarchy mainly targets task partitioning (selection vs. execution) rather than asset-structural partitioning, and therefore remains limited in capturing cross-asset relationships. By contrast, our hierarchical design is tailored for asset classification and cross-asset relationship modeling, with explicit division of roles between levels. This ensures that the hierarchical objectives are tightly coupled with market structure, enabling more effective operation under non-stationary environments.

To more intuitively demonstrate the current research results on extracting potential connections between assets, we summarize the relevant studies and present the results in [Table 1](#).

3 Definition

This section includes definitions of financial markets and portfolios, and relevant mathematical definitions related to market transactions. It provides the theoretical basis for our work.

3.1 Financial Market

The financial market represents a complex ecosystem in which a wide range of instruments – such as equities, fixed income assets, and certificates of deposit – are continuously traded with the aim of generation of returns. This study concentrates on the U.S. equity market, which is distinguished by its comprehensive regulatory framework and substantial liquidity, rendering it one of the leading markets worldwide in terms of capitalization and the scale of investor participation [Harris and Ravenscraft \(1991\)](#).

3.2 Portfolio

Portfolio management constitutes a systematic investment process aimed at maximizing returns through the optimization of asset allocation. Consider an investor selecting m stocks, where $m > 0$, with the portfolio adjust closing price vector at time t represented by the $m \times 1$ column vector

$$\mathbf{v}_{t-1} = [v_{1,t-1}, v_{2,t-1}, \dots, v_{m-1,t-1}, v_{m,t-1}]^T.$$

For analytical purposes, the investment horizon is partitioned into F discrete intervals, each associated with a period $t \in \mathbb{N}$. A period t begins immediately after t and concludes at $t + 1$, corresponding to the open-closed interval $(t, t + 1]$. The relative price vector of the portfolio, denoted as \mathbf{z}_t and having dimension $1 \times m$, is defined as a function of \mathbf{v}'_t (the portfolio price vector at the beginning of period t) and \mathbf{v}_t (the price vector at the end of period t):

$$\mathbf{z}_t = \mathbf{v}_t \oslash \mathbf{v}_{t-1},$$

where \oslash indicates element-wise division. In view of arguments suggesting that upward price movements should not be regarded as a source of risk [Rollinger and Hoffman \(2013\)](#), this study utilizes the asset Sortino ratio $\mathbf{z}_{Sortino}$ [Rollinger and Hoffman \(2013\)](#), a $1 \times m$ vector, to quantify asset risk. The Sortino ratio incorporates downside standard deviation, reflecting the perspective that only adverse volatility represents true risk [Rollinger and Hoffman \(2013\)](#). Unlike the Sharpe ratio, which penalizes both upside and downside volatility, the Sortino ratio concentrates exclusively on downside deviation, thereby providing a risk measure that better aligns with investor preferences and the asymmetric nature of financial return distributions [Rollinger and Hoffman \(2013\)](#). This property makes it particularly suitable for portfolio optimization and for integration into reinforcement learning frameworks, where distinguishing harmful volatility from favorable gains is critical for designing effective risk-aware allocation strategies [Rollinger and Hoffman \(2013\)](#). Formally, the asset Sortino ratio $\mathbf{z}_{Sortino}$ measures the excess return per unit of downside risk and is defined as

$$\mathbf{z}_{Sortino} = \frac{\mathbb{E}[\log_2(\mathbf{z}_t) - r_A]}{\sqrt{\frac{1}{j} \sum_{\log_2(\mathbf{z}_t) < r_A}^j (\log_2(\mathbf{z}_t) - r_A)^2}},$$

where r_A denotes the minimum acceptable logarithmic return with base 2, specified as the daily logarithmic risk-free rate r_A in this study. The $\mathbb{E}[\cdot]$ denotes the expectation. The index j corresponds to the number of periods during which the daily logarithmic return of an asset falls below this threshold. For $\mathbf{z}_{Sortino}$, larger values indicate stronger potential for asset appreciation.

For mitigating decision complexity, capturing structural heterogeneity, and adapting to evolving market conditions, this work applies K-means clustering [Jin and Han \(2010\)](#) for dynamic asset classification. K-means is an unsupervised learning algorithm that partitions the dataset into k disjoint clusters by minimizing intra-cluster variance:

$$\arg \min_C \sum_{i=1}^k \sum_{\log_2(\mathbf{v}_{j,t-1}) \in C_i} \|\log_2(\mathbf{v}_{j,t-1}) - \log_2(\mathbf{v}_{a_i,t-1})\|_1^2,$$

where $\mathbf{v}_{a_i,t-1}$ denotes the adjusted closing price vector of asset a_i , which serves as the representative (centroid) of cluster C_i , and $\|\cdot\|_1$ is the L_1 norm, measuring the sum of absolute changes in portfolio weights and thus quantifying the total volume of reallocation. The parameter k is predetermined; in this study $k = 2$, corresponding to two asset groups. As noted by Fama and French [Fama and French \(1993\)](#),

excessive stratification may fragment portfolios and lead to unstable estimates, which further justifies our parsimonious two-group design. The algorithm iteratively alternates between assigning data points to the nearest centroid and recalculating centroids as the mean of the assigned points, until assignments stabilize or the objective function converges. To balance sensitivity to regime shifts with computational tractability, clustering is re-executed every 75 trading days, which approximately aligns with a quarterly cycle [Camanho et al. \(2022\)](#); [Kuhn and Luenberger \(2010\)](#).

The adoption of K-means clustering confirms three distinct benefits. First, it offers a straightforward and computationally efficient approach for categorizing large-scale asset sets [Cai et al. \(2025\)](#). Second, by incorporating Sortino ratio features, the classification emphasizes risk-adjusted returns rather than raw price movements [Jin and Han \(2010\)](#). Third, periodic re-execution enables dynamic restructuring of asset clusters in response to market evolution, thereby strengthening the robustness and adaptability of the overall portfolio optimization process [Namitha and Santhosh Kumar \(2020\)](#).

After applying K-means clustering, the result is expressed as $C = \{C^{(1)}, C^{(2)}\}$, which partitions the asset universe into two mutually exclusive subsets. To embed this clustering outcome within the hierarchical reinforcement learning framework, binary masks $m_{i,t}^{(1)}$ and $m_{i,t}^{(2)}$ are introduced for each cluster, defined as

$$\begin{aligned} \mathbf{m}_{i,t-1}^{(1)} &= \begin{cases} 1, & \text{if asset } i \in C_{i,t-1}^{(1)} \\ 0, & \text{otherwise} \end{cases} \\ \mathbf{m}_{i,t-1}^{(2)} &= \begin{cases} 1, & \text{if asset } i \in C_{i,t-1}^{(2)} \\ 0, & \text{otherwise} \end{cases} \end{aligned}$$

where $\mathbf{m}_t^{(1)}$ and $\mathbf{m}_t^{(2)}$ denote complementary masks of dimension $1 \times m$, ensuring that only the assets associated with their respective clusters remain active. These masks are then employed to guide the lower-level agents, thereby constraining intra-group allocation to assets within each dynamically identified group. Using $\mathbf{m}_{i,t-1}^{(1)}$, $\mathbf{m}_{i,t-1}^{(2)}$, and the price vector \mathbf{v}_{t-1} , the masked price vectors $\mathbf{v}_{t-1}^{(1)}$ and $\mathbf{v}_{t-1}^{(2)}$ corresponding to Group 1 and Group 2 are obtained as

$$\begin{aligned} \mathbf{v}_{t-1}^{(1)} &= \mathbf{v}_{t-1} \odot \mathbf{m}_{t-1}^{(1)} \\ \mathbf{v}_{t-1}^{(2)} &= \mathbf{v}_{t-1} \odot \mathbf{m}_{t-1}^{(2)} \end{aligned}$$

where \odot denotes the *Hadamard product* [Horn \(1990\)](#). The portfolio price history over the most recent n periods is represented by the matrix \mathbf{q}_{t-1} , an $m \times n$ matrix defined as

$$\mathbf{q}_{t-1} = [\mathbf{v}_{t-n}, \mathbf{v}_{t-n+1}, \dots, \mathbf{v}_{t-2}, \mathbf{v}_{t-1}].$$

Analogously, the price matrices $\mathbf{q}_{t-1}^{(1)}$ and $\mathbf{q}_{t-1}^{(2)}$ corresponding to Groups 1 and 2 are given by

$$\begin{aligned} \mathbf{q}_{t-1}^{(1)} &= \mathbf{q}_{t-1} \odot \mathbf{m}_{t-1}^{(1)} \\ \mathbf{q}_{t-1}^{(2)} &= \mathbf{q}_{t-1} \odot \mathbf{m}_{t-1}^{(2)} \end{aligned}$$

Based on the stock price matrix $\mathbf{q}_{t-1}^{(1)}, \mathbf{q}_{t-1}^{(2)}$ and the mask $\mathbf{m}_{t-1}^{(1)}, \mathbf{m}_{t-1}^{(2)}$, we obtain the logarithmic relative price matrix $\mathbf{lzq}_{t-1}^{(1)}, \mathbf{lzq}_{t-1}^{(2)}$:

$$\begin{aligned}\mathbf{lzq}_{t-1}^{(1)} &= \log_2 \left(\mathbf{q}_{t-1}^{(1)} \oslash \mathbf{q}_{t-2}^{(1)} \right) \\ \mathbf{lzq}_{t-1}^{(2)} &= \log_2 \left(\mathbf{q}_{t-1}^{(2)} \oslash \mathbf{q}_{t-2}^{(2)} \right).\end{aligned}$$

Within the portfolio, the allocation of capital at time t is represented by the weight vector $\boldsymbol{\omega}_{t-1}$, defined as

$$\boldsymbol{\omega}_{t-1} = [\omega_{1,t-1}, \omega_{2,t-1}, \dots, \omega_{m-1,t-1}, \omega_{m,t-1}]^T,$$

which is an $m \times 1$ vector. The initial weight vector is specified as the zero vector of dimension $m \times 1$, indicating that the initial endowment is entirely allocated to cash. At any time t , the portfolio weights satisfy the budget constraint

$$\sum_{i=1}^m \omega_{i,t-1} = 1.$$

Correspondingly, the group-specific allocations are denoted by $\boldsymbol{\omega}_{t-1}^{(1)}$ and $\boldsymbol{\omega}_{t-1}^{(2)}$, defined through the masking mechanism:

$$\begin{aligned}\boldsymbol{\omega}_{t-1}^{(1)} &= \boldsymbol{\omega}_{t-1} \odot \mathbf{m}_{t-1}^{(1)} \\ \boldsymbol{\omega}_{t-1}^{(2)} &= \boldsymbol{\omega}_{t-1} \odot \mathbf{m}_{t-1}^{(2)} \\ 1 &= \sum_{j=1}^m \omega_{j,t-1}^{(1)} + \sum_{i=1}^m \omega_{j,t-1}^{(2)} + \omega_{t-1}^{(f)},\end{aligned}$$

where $\omega_{t-1}^{(f)}$ is the weight of risk free asset at time t . The portfolio value prior to trading at time t , denoted as p_{t-1} , is determined jointly with the share vector \mathbf{sh}_{t-1} , which represents the number of shares hold across assets. These quantities are obtained as

$$\begin{aligned}\mathbf{sh}_{t-1} &= \mathbf{sh}_{t-1}^{(1)} + \mathbf{sh}_{t-1}^{(2)}, \\ p_{t-1}^{(1)} &= \mathbf{sh}_{t-1}^{(1)T} \mathbf{v}_{t-1}^{(1)} + h_{t-1}^{(1)} \\ \mathbf{sh}_{t-1}^{(1)} &= \left[p_{t-1}^{(1)'} \boldsymbol{\omega}_{t-1}^{(1)'} \oslash \mathbf{v}_{t-1}^{(1)'} \right] \\ p_{t-1}^{(2)} &= \mathbf{sh}_{t-1}^{(2)T} \mathbf{v}_{t-1}^{(2)} + h_{t-1}^{(2)}, \\ \mathbf{sh}_{t-1}^{(2)} &= \left[p_{t-1}^{(2)'} \boldsymbol{\omega}_{t-1}^{(2)'} \oslash \mathbf{v}_{t-1}^{(2)'} \right] \\ p_{t-1}^{(f)} &= p_{t-1}' \omega_{t-1}^{(f)'} 2^{r_A} \\ p_{t-1} &= p_{t-1}^{(1)} + p_{t-1}^{(2)} + p_{t-1}^{(f)}\end{aligned}$$

where, $\mathbf{sh}_{t-1}^{(1)}$, $\mathbf{sh}_{t-1}^{(2)}$, $h_{t-1}^{(1)}$, and $h_{t-1}^{(2)}$ denote the share holdings and residual cash for Groups 1 and 2, respectively, at time t . Portfolio values of Group 1, 2 and risk free asset at time t are denoted as $p_{t-1}^{(1)}$, $p_{t-1}^{(2)}$ and $p_{t-1}^{(f)}$. Similarly, $p_{t-1}^{(1)'}$, $p_{t-1}^{(2)'}$, $p_{t-1}^{(f)'}$ and $\omega_{t-1}^{(1)'}$, $\omega_{t-1}^{(2)'}$, $\omega_{t-1}^{(f)'}$ denote portfolio values and weight vector of Groups 1, 2 and risk free asset at beginning of period $t-1$. The operator \oslash specifies element-wise division, while the floor operator $\lfloor \cdot \rfloor$ enforces integer rounding of the number of shares by truncation. Refer to Figure 1 for a comprehensive illustration of the transaction mechanism. At the end of period $t-1$ (i.e., at time t), the price vectors, portfolio values, and allocation weights of the two groups are denoted by $\mathbf{v}_{t-1}^{(1)}$, $\mathbf{v}_{t-1}^{(2)}$, $p_{t-1}^{(1)}$, $p_{t-1}^{(2)}$, $\omega_{t-1}^{(1)}$, and $\omega_{t-1}^{(2)}$, respectively. Once transactions at time t are executed, the updated states of the system are represented as $\mathbf{v}_t^{(1)'}$, $\mathbf{v}_t^{(2)'}$, $p_t^{(1)'}$, $p_t^{(2)'}$, $\omega_t^{(1)'}$, and $\omega_t^{(2)'}$. The portfolio is then maintained without additional rebalancing until the conclusion of period t .

Each transaction occurs instantaneously at the decision point. Upon completion, the group-specific price vectors $\mathbf{v}_{t-1}^{(1)}$ and $\mathbf{v}_{t-1}^{(2)}$ are updated to $\mathbf{v}_t^{(1)'}$ and $\mathbf{v}_t^{(2)'}$, the group values $p_{t-1}^{(1)}$ and $p_{t-1}^{(2)}$ become $p_t^{(1)'}$ and $p_t^{(2)'}$, and the weight vectors $\omega_{t-1}^{(1)}$ and $\omega_{t-1}^{(2)}$ transform into $\omega_t^{(1)'}$ and $\omega_t^{(2)'}$, all reflecting the newly determined investment strategy. For analytical tractability, this study assumes that trading activity does not influence asset prices, i.e., $\mathbf{v}_{t-1}^{(1)} = \mathbf{v}_t^{(1)'}$ and $\mathbf{v}_{t-1}^{(2)} = \mathbf{v}_t^{(2)'}$ [Jiang et al. \(2017\)](#). Consequently, the price vectors at the start of period t are represented as $\mathbf{v}_t^{(1)'}$ and $\mathbf{v}_t^{(2)'}$. The initial group values $p_t^{(1)'}$ and $p_t^{(2)'}$ at the beginning of period t are expressed as

$$\begin{aligned} p_t^{(1)'} &= u_t^{(1)} p_{t-1}^{(1)} \\ p_t^{(2)'} &= u_t^{(2)} p_{t-1}^{(2)}, \end{aligned}$$

where $u_t^{(1)}$ and $u_t^{(2)}$ denote the proportional reductions in group values at time t due to transaction costs.

Transaction costs are deducted from group values, denoted by $Cost_t^{(1)}$ and $Cost_t^{(2)}$. The fee structure is formalized as:

$$\begin{aligned} Cost_t^{(1)} &= cs p_{t-1}^{(1)} \left\| \omega_{t-1}^{(1)} - \omega_t^{(1)'} \right\|_1 \\ Cost_t^{(2)} &= cs p_{t-1}^{(2)} \left\| \omega_{t-1}^{(2)} - \omega_t^{(2)'} \right\|_1, \end{aligned}$$

where cs represents the transaction cost rate. Following [Jiang et al. \(2017\)](#), the transaction cost rate c is fixed at 0.001. After rebalancing, the residual cash

holdings $h_t^{(1)}$ and $h_t^{(2)}$ that remain unallocated to equities are expressed as

$$h_t^{(1)} = \begin{cases} \frac{(h_{t-1}^{(1)} + h_{t-1}^{(2)}) \cdot \sum_{i=1}^m \omega_{i,t-1}^{(1)}}{\sum_{i=1}^m \omega_{i,t-1}^{(1)} + \sum_{i=1}^m \omega_{i,t-1}^{(2)}} - p_t^{(1)\prime} + p_{t-1}^{(1)}, & \text{if } t \geq 2 \\ \frac{p_0 \cdot \sum_{i=1}^m \omega_{i,t-1}^{(1)}}{\sum_{i=1}^m \omega_{i,t-1}^{(1)} + \sum_{i=1}^m \omega_{i,t-1}^{(2)}} - p_t^{(1)\prime} + p_{t-1}^{(1)}, & \text{if } t = 1 \end{cases},$$

$$h_t^{(2)} = \begin{cases} \frac{(h_{t-1}^{(1)} + h_{t-1}^{(2)}) \cdot \sum_{i=1}^m \omega_{i,t-1}^{(2)}}{\sum_{i=1}^m \omega_{i,t-1}^{(1)} + \sum_{i=1}^m \omega_{i,t-1}^{(2)}} - p_t^{(2)\prime} + p_{t-1}^{(2)}, & \text{if } t \geq 2 \\ \frac{p_0 \cdot \sum_{i=1}^m \omega_{i,t-1}^{(2)}}{\sum_{i=1}^m \omega_{i,t-1}^{(1)} + \sum_{i=1}^m \omega_{i,t-1}^{(2)}} - p_t^{(2)\prime} + p_{t-1}^{(2)}, & \text{if } t = 1 \end{cases},$$

where p_0 denotes the initial portfolio value. If any allocation leads to $h_t^{(1)} < 0$ or $h_t^{(2)} < 0$, the transaction is proportionally scaled down to guarantee non-negativity of the cash balance, i.e., $h_t^{(1)}, h_t^{(2)} \geq 0$. This mechanism prohibits debt accumulation and enforces that all asset positions are backed by available capital. The same feasibility constraint is consistently applied across all settings to ensure a fair and comparable evaluation.

The value of the portfolio at the beginning of period t , denoted p_t' , is given by

$$p_t^{(1)\prime} = u_t^{(1)} p_{t-1}^{(1)} = \begin{cases} \frac{(h_{t-1}^{(1)} + h_{t-1}^{(2)}) \cdot \sum_{i=1}^m \omega_{i,t-1}^{(1)}}{\sum_{i=1}^m \omega_{i,t-1}^{(1)} + \sum_{i=1}^m \omega_{i,t-1}^{(2)}} - h_t^{(1)} + p_{t-1}^{(1)}, & \text{if } t \geq 2 \\ \frac{p_0 \cdot \sum_{i=1}^m \omega_{i,t-1}^{(1)}}{\sum_{i=1}^m \omega_{i,t-1}^{(1)} + \sum_{i=1}^m \omega_{i,t-1}^{(2)}} - h_t^{(1)} + p_{t-1}^{(1)}, & \text{if } t = 1 \end{cases}.$$

$$p_t^{(2)\prime} = u_t^{(2)} p_{t-1}^{(2)} = \begin{cases} \frac{(h_{t-1}^{(1)} + h_{t-1}^{(2)}) \cdot \sum_{i=1}^m \omega_{i,t-1}^{(2)}}{\sum_{i=1}^m \omega_{i,t-1}^{(1)} + \sum_{i=1}^m \omega_{i,t-1}^{(2)}} - h_t^{(2)} + p_{t-1}^{(2)}, & \text{if } t \geq 2 \\ \frac{p_0 \cdot \sum_{i=1}^m \omega_{i,t-1}^{(2)}}{\sum_{i=1}^m \omega_{i,t-1}^{(1)} + \sum_{i=1}^m \omega_{i,t-1}^{(2)}} - h_t^{(2)} + p_{t-1}^{(2)}, & \text{if } t = 1 \end{cases}.$$

The transaction return in period t is quantified through the base-2 logarithmic rate of return φ_t , defined as

$$\varphi_t = \log_2 \left(\frac{p_t}{p_{t-1}} \right)$$

$$\varphi_t^{(1)} = \log_2 \left(\frac{p_t^{(1)}}{p_{t-1}^{(1)}} \right),$$

$$\varphi_t^{(2)} = \log_2 \left(\frac{p_t^{(2)}}{p_{t-1}^{(2)}} \right)$$

where $\varphi_t^{(1)}$ and $\varphi_t^{(2)}$ denote group-specific returns. This iterative process continues for all periods, and the final portfolio value p_f is expressed as

$$p_f = p_0 \cdot 2^{\sum_{t=1}^F \varphi_t},$$

with F indicating the total number of investment periods and φ_0 is the initial capital. In this study, the initial capital is set to 1 million dollars.

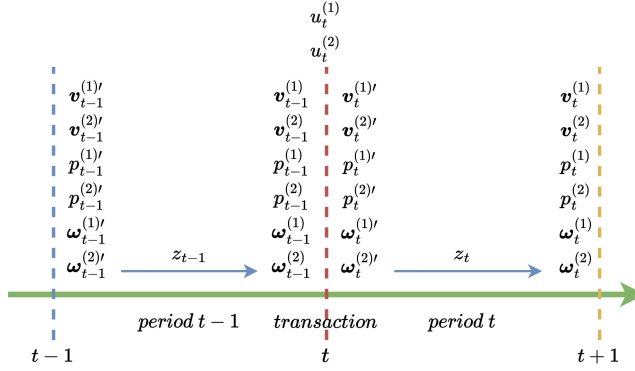


Fig. 1 Transaction flow. At the end of time $t-1$ (equivalently, at the beginning of trading period t), the system state is described by the price vectors $\mathbf{v}_{t-1}^{(1)}$ and $\mathbf{v}_{t-1}^{(2)}$, the group values $p_{t-1}^{(1)}$ and $p_{t-1}^{(2)}$, and the allocation weights $\omega_{t-1}^{(1)}$ and $\omega_{t-1}^{(2)}$. The proportional adjustments in group values induced by the rebalancing decision at time t are denoted by $u_t^{(1)}, u_t^{(2)} \in [0, 1]$. Immediately after rebalancing, the updated state variables become $\mathbf{v}_t^{(1)'}, \mathbf{v}_t^{(2)'}, p_t^{(1)'}, p_t^{(2)'}, \omega_t^{(1)'}$, and $\omega_t^{(2)'}$, which remain unchanged throughout period t . At the end of period t , the realized market state is expressed as $\mathbf{v}_t^{(1)}, \mathbf{v}_t^{(2)}, p_t^{(1)}, p_t^{(2)}, \omega_t^{(1)}$, and $\omega_t^{(2)}$. The relative change in asset prices during period t is captured by the relative price vector \mathbf{z}_t .

3.3 Assumptions

The analysis is based on two foundational assumptions, denoted as A1 and A2.

A1: The market possesses sufficient liquidity to enable the prompt execution of each transaction.

A2: Transactions are assumed to have no impact on stock prices.

According to Assumption A1, if a stock exhibits sufficiently high liquidity such that its trading volume exceeds the required execution size, all proposed trades can be executed without delay. Assumption A1 is essential to the framework, as daily market volume cannot be forecasted with precision. In practical markets, large transaction volumes can influence stock prices because both buying and selling activities convey investors' sentiments and are reflected in price fluctuations. Therefore, Assumption A2 is introduced to abstract from this price-impact effect and maintain model tractability. Taken together, these two assumptions hold reasonably well when the selected stocks exhibit sufficiently high liquidity [Jiang et al. \(2017\)](#).

Although a transaction cost of 0.1% per transaction is incorporated in the experimental design to simulate basic market frictions [Jiang et al. \(2017\)](#), several critical aspects of real-world trading—such as slippage, order book depth constraints, and market impact—remain insufficiently modeled [Kyle \(1985\)](#). Under such conditions, applying the proposed strategy in live trading environments may result in execution price deviations [Kyle \(1985\)](#) and partial fills [Lo et al. \(2002\)](#), which significantly deteriorate the realized returns compared to backtests results. Furthermore, the multi-asset coordinated rebalancing paths learned by the agent during training may become infeasible due to real-world execution constraints, thereby impairing portfolio optimization

effectiveness and overall strategy stability. Nevertheless, the proposed framework is equipped to jointly capture both long-term trends and short-term market dynamics, enabling it to adaptively modulate trading frequency based on prevailing market regimes. This multi-timescale perception mechanism offers greater flexibility and robustness compared to strategies relying solely on single-horizon signals, contributing to improved resilience against execution errors and performance degradation induced by market frictions [Wei et al. \(2021\)](#). It is worth noting that, although these idealized assumptions may lead to systematic overestimation of the absolute performance across all evaluated strategies, each approach—ranging from traditional rule-based baselines to alternative reinforcement learning frameworks—is assessed under the same experimental conditions. Therefore, the simplification applies uniformly across methods, ensuring the relative fairness of performance comparisons and preserving the validity of the observed inter-strategy rankings.

4 Framework of DRL

4.1 Overall Framework

The proposed structure combines the continuous-control capability of the Deep Deterministic Policy Gradient (DDPG) [Lillicrap et al. \(2015a\)](#) algorithm with the task-decomposition advantage of HRL [Barto and Mahadevan \(2003b\)](#). The upper-level agent provides stable global representations and guidance, while the lower-level agents perform fine-grained allocation within dynamically defined asset groups. Through this design, the framework establishes coherent linkages between global and local perspectives, thereby enhancing feature utilization, allocation granularity, and interpretability. The overall workflow of the proposed architecture is illustrated in Figure 2.

4.1.1 Hierarchical Reinforcement Learning Design

Hierarchical reinforcement learning decomposes and coordinates complex tasks through the cooperation of upper- and lower-level agents [Barto and Mahadevan \(2003b\)](#). In the proposed design, the upper-level agent (Agent 0) extracts global market signals and is then kept fixed to provide a stable supervisory interface, while the lower-level agents (Agent 1 and Agent 2) operate under dynamic masking constraints to allocate weights across ordinary and high-quality asset groups. This structure enables simultaneous modeling of global and local decision information, thereby enhancing representational richness and refining allocation granularity.

4.1.2 Hierarchical Decision Mechanism

Leveraging dynamic asset grouping and allocation process is explicitly integrated into a unified hierarchical reinforcement learning framework. Unlike rule-based subset updates [Jiang et al. \(2023\); Peng et al. \(2024b\); Zouaghia et al. \(2025\); Ashrafpour et al. \(2023\)](#) or implicit black-box selections [Jiang et al. \(2017\); Yang \(2023\)](#), the mechanism enforces explicit information flow and cross-layer consistency constraints.

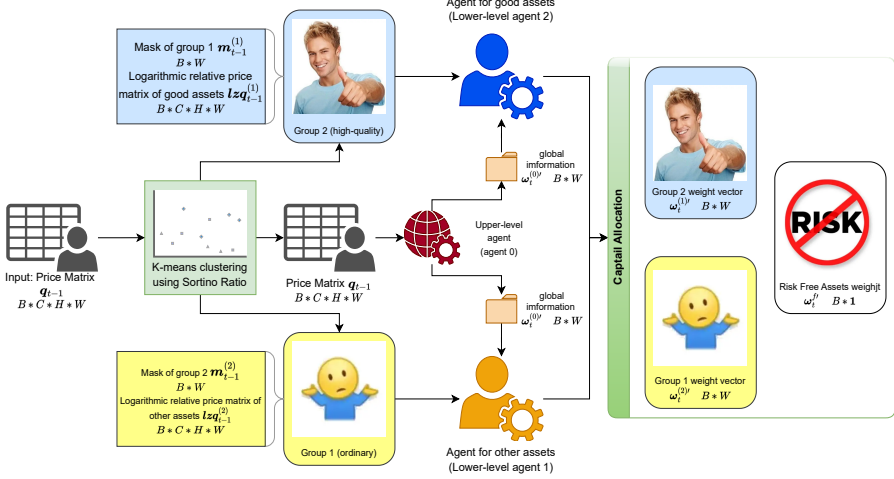


Fig. 2 Workflow of the proposed architecture. The state representation is first processed through dynamic clustering and masking, after which the upper-level agent extracts global signals and the lower-level agents perform intra-group allocation. A fusion mechanism then integrates the outputs to produce the final portfolio weights, ensuring that alongside concentrated investment in high-quality assets, the inclusion of remaining assets provides diversification benefits that reduce overall portfolio risk [Sharpe \(1964\)](#).

This design improves interpretability of the decision process and ensures coherent coordination between global and local decision modules.

4.2 State, Action and Reward

In reinforcement learning (RL), the interaction between the agent and the environment follows a closed-loop process, as illustrated in Figure 3. At each decision step t , the agent observes the environment through the state s_t , generates an action a_t based on its policy, and applies this action to the environment. The environment then responds by updating the system dynamics and returning both a new state s_{t+1} and a scalar reward r_{t+1} . This iterative process allows the agent to optimize its policy so as to maximize cumulative rewards over time [De Asis et al. \(2018\)](#). In the context of portfolio optimization, the environment corresponds to the financial market, the state encapsulates observable market information and portfolio status, the action represents allocation decisions across assets, and the reward reflects investment performance [Jiang et al. \(2017\)](#). The following subsections elaborate on the detailed design of state, action, and reward in this study.

In reinforcement learning, the state s_t refers to the complete information observed by the agent from the environment at time t , which provides the basis for decision-making. As illustrated in the standard agent–environment interaction loop, the environment updates the portfolio value after receiving the action a_t and returns the new state s_{t+1} together with the immediate reward r_{t+1} . The construction of the state thus determines the agent’s perception of the market environment [Mnih et al. \(2015\)](#).

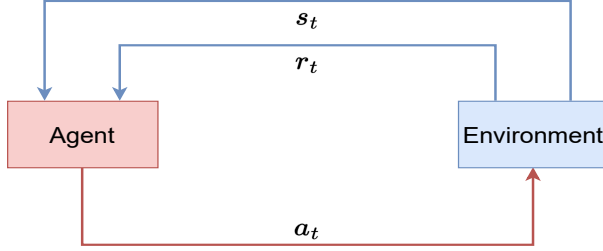


Fig. 3 [Closed-loop interaction.] Closed-loop interaction between agent and environment in reinforcement learning, where the agent observes the state s_t , takes action a_t , and receives the reward r_t together with the next state s_{t+1} .

In the portfolio optimization problem, the environment corresponds to the financial market, and the state should capture market dynamics, portfolio positions, and structural constraints. In this study, the state at time t is defined as

$$s_t = \{q_{t-1}, \mathbf{sh}_{t-1}^{(1)}, \mathbf{sh}_{t-1}^{(2)}, \mathbf{m}_{t-1}^{(1)}, \mathbf{m}_{t-1}^{(2)}\},$$

where

- $q_{t-1} \in \mathbb{R}^{m \times n}$: the price history matrix of the past n days, reflecting the temporal evolution of the market;
- $\mathbf{sh}_{t-1}^{(1)}, \mathbf{sh}_{t-1}^{(2)}$: the portfolio positions of the two asset groups *before the current transaction*, ensuring that decisions are conditioned on existing holdings rather than reinitialized at each step;
- $\mathbf{m}_{t-1}^{(1)}, \mathbf{m}_{t-1}^{(2)} \in \{0, 1\}^m$: binary masks generated by dynamic clustering, indicating the tradable subsets at time t .

This state representation is shared across all three agents – one upper-level agent and two lower-level agents—thereby providing a unified market perception. Such a shared-state design ensures consistent information flow throughout the hierarchical framework, while allowing each agent to concentrate on its designated decision-making responsibility [Lowe et al. \(2017\)](#). By jointly encoding temporal information, path-dependent holdings, and dynamically evolving market structures, this formulation enhances adaptability and robustness in non-stationary financial environments.

In reinforcement learning, the action a_t denotes the agent's policy output under state s_t , which directly influences portfolio evolution and determines future returns. In the portfolio optimization setting, the action corresponds to the allocation weights assigned to assets. At time t , the actions $a_t^{(0)}$ and $a_t^{(1)}$ is defined as

$$\begin{aligned} a_t^{(0)} &= \{\boldsymbol{\omega}_t^{(1)'}\} \\ a_t^{(1)} &= \{\boldsymbol{\omega}_t^{(2)'}\}. \end{aligned}$$

Here, $\omega 1'_t$ is nonzero only for assets indicated by $m1_t$, and $\omega 2'_t$ is nonzero only for assets indicated by $m2_t$. Together, they satisfy the budget constraint:

$$\sum_{j=1}^m \omega_{j,t}^{(1)'} + \sum_{j=1}^m \omega_{j,t}^{(2)'} + \omega_t^{f'} = 1.$$

This formulation decomposes the global allocation problem into two structured subproblems, allowing the agent to optimize allocations within each group while maintaining overall capital conservation.

In reinforcement learning, the reward R_t provides the immediate feedback signal that drives policy optimization [De Asis et al. \(2018\)](#). In the proposed hierarchical framework, the asset universe is dynamically partitioned into two subsets through K-means clustering [Jin and Han \(2010\)](#), where the clustering is periodically executed on rolling windows of asset returns to capture regime shifts and structural changes in the market. For each group $i \in \{1, 2\}$, the instantaneous reward $R_t^{(i)}$ is based on the logarithmic return $\log_2 \left(\frac{p_t^{(i)}}{p_{t-1}^{(i)}} \right)$. To stabilize the learning process, this base reward $R_t^{(i)}$ is further defined as

$$R_t^{(i)} = \begin{cases} \kappa \cdot \log_2 \left(\frac{p_t^{(i)}}{p_{t-1}^{(i)}} \right), & N_{t-1} < 2, \\ \kappa \cdot \left(\log_2 \left(\frac{p_t^{(i)}}{p_{t-1}^{(i)}} \right) - \beta_{t-1}^{adj} \cdot \sigma_{t-1}^{(i)} \right), & N_{t-1} \geq 2, \end{cases}$$

where κ is a positive scaling coefficient introduced to amplify the reward signal, ensuring sufficient gradient magnitude during training and stabilizing policy optimization [Mnih et al. \(2015\)](#). The term $\sigma_{t-1}^{(i)}$ denotes the standard deviation of historical log-returns for group i at time t , and N_{t-1} represents the number of past observations available at time t . The adaptive risk-aversion coefficient β_{t-1}^{adj} is then defined as

$$\beta_{t-1}^{adj} = \beta \cdot \frac{N_{t-1}}{\eta},$$

where β is a fixed hyperparameter set to 0.2 in this study and η is a normalization constant representing the baseline number of observations [Moody and Saffell \(2001\)](#). Here, β serves as the baseline risk-aversion factor that regulates the strength of volatility penalization in the reward function: a smaller β prioritizes return maximization with limited regard for risk, whereas a larger β enforces more conservative behavior by amplifying the influence of volatility [Bisi et al. \(2019\)](#). Multiplication by $\frac{N_{t-1}}{\eta}$ allows the overall coefficient β_{t-1}^{adj} to increase as the number of observations grows, thereby reducing the weight of risk penalties when estimates are noisy in early stages and strengthening robustness as more reliable information becomes available [Bisi et al. \(2019\)](#).

The group-wise reward formulation establishes a one-to-one correspondence between each reward signal and the agent responsible for its designated asset group. Specifically, $R_t^{(1)}$ is assigned to agent 1 managing asset group 1, while $R_t^{(2)}$ is assigned to agent 2 managing asset group 2. This design ensures that the optimization objectives remain consistent with the structural decomposition of the market, while simultaneously enhancing interpretability, since the contribution of each asset group to policy learning can be explicitly identified.

4.3 Clustering and Mask Mechanism

To introduce structured constraints into the hierarchical reinforcement learning framework, this study applies the K-means algorithm [Jin and Han \(2010\)](#) to partition assets into two groups: **Group 1 (high-quality assets)** and **Group 2 (ordinary assets)**. For each group, a binary mask vector is constructed to restrict the input space of the lower-level agents. For the asset universe at time t , the clustering result is denoted as $C_{t-1} = \{C_{1,t-1}, C_{2,t-1}\}$. The corresponding masks are defined as

$$\begin{aligned}\mathbf{m}_{j,t-1}^{(1)} &= \begin{cases} 1, & \text{if asset } j \text{ belongs to Group 1 (high-quality)} \\ 0, & \text{otherwise} \end{cases} \\ \mathbf{m}_{j,t-1}^{(2)} &= \begin{cases} 1, & \text{if asset } j \text{ belongs to Group 2 (ordinary)} \\ 0, & \text{otherwise} \end{cases}\end{aligned}$$

At any time t , the masks are complementary, satisfying $\mathbf{m}_{t-1}^{(1)} + \mathbf{m}_{t-1}^{(2)} = \mathbf{1}$. Based on these masks, the subset input logarithmic return matrix matrices $\mathbf{z}_{t-1}^{(1)}, \mathbf{z}_{t-1}^{(2)}$ are obtained:

$$\begin{aligned}\mathbf{z}_{t-1}^{(1)} &= \mathbf{z}_{t-1} \odot \mathbf{m}_{t-1}^{(1)} \\ \mathbf{z}_{t-1}^{(2)} &= \mathbf{z}_{t-1} \odot \mathbf{m}_{t-1}^{(2)} \\ \mathbf{z}_{t-1} &= \log_2 (\mathbf{q}_{t-1} \oslash \mathbf{q}_{t-2})\end{aligned}$$

Correspondingly, the lower-level agents output the group-specific weight vectors $\boldsymbol{\omega}_{t-1}^{(1)}$ and $\boldsymbol{\omega}_{t-1}^{(2)}$, which allocate capital within Group 1 and Group 2, respectively:

$$\begin{aligned}\boldsymbol{\omega}_t^{(1)'} &= \boldsymbol{\omega}_t' \odot \mathbf{m}_{t-1}^{(1)} \\ \boldsymbol{\omega}_t^{(2)'} &= \boldsymbol{\omega}_t' \odot \mathbf{m}_{t-1}^{(2)}\end{aligned}$$

Through this clustering and mask mechanism, the model conducts group-wise learning, ensuring that each lower-level agent operates strictly within its designated subset of assets. This design reduces the complexity of the action space and establishes a clear structural constraint for subsequent weight fusion and global decision-making [Walauskis and Khoshgoftaar \(2025\)](#); [Peng et al. \(2025\)](#).

4.4 DDPG Framework

DDPG is a canonical actor–critic based deep reinforcement learning approach that is suitable for control tasks in continuous action spaces [Lillicrap et al. \(2015a\)](#). In this framework, the actor network outputs deterministic actions, such as portfolio weights, while the critic network evaluates state–action pairs and updates parameters through policy gradients. Because DDPG directly models continuous numerical outputs, it aligns with portfolio optimization, where weight adjustments are inherently continuous.

4.5 Actor–Critic Network Structure

The upper-level agent employs a transformer-based architecture validated in prior financial applications [Ren et al. \(2025\)](#). This choice underscores that our contribution lies in structural innovation, while relying on established networks for function approximation. This structure employs a transformer-based model that effectively captures temporal dependencies in financial time series and cross-sectional correlations among assets [Vaswani et al. \(2017\)](#). Compared with conventional recurrent or convolutional networks, the transformer-based architecture exhibits stronger capability in extracting global market features. The spatial interaction and hierarchical relationship between the upper-level and lower-level agents are illustrated in Figure 2. As depicted, clustered and masked states are processed by the upper-level and lower-level agents in parallel, and a fusion module integrates their outputs into the final portfolio weights, preserving both focus and diversification [Sharpe \(1964\)](#). As illustrated in Fig. 4, the hierarchical reinforcement learning framework comprises an upper-level agent and two lower-level agents that interact through structured information exchange. It is particularly noteworthy that the upper-level agent directly receives the complete price information \mathbf{q}_{t-1} , enabling it to capture inter-asset correlation structures and price dynamics. Its implicit output, denoted as $\boldsymbol{\omega}_t^{(0) \prime}$, serves as a global guidance signal that encapsulates this information and is subsequently provided to the lower-level agents for coherent coordination. In contrast, the lower-level agents operate on logarithmic return matrices under mask constraints $\mathbf{z}_{t-1}^{(1)}, \mathbf{z}_{t-1}^{(2)}$, masks $\mathbf{m}_{t-1}^{(1)}, \mathbf{m}_{t-1}^{(2)}$, and information $\boldsymbol{\omega}_t^{(0) \prime}$ obtained from the upper-level agent. The focus of the lower-level agents is confined to intra-group weight allocation, which ensures coherence between global objectives and local optimization processes. As a result, they lack the capacity to represent global cross-asset relationships. Through this hierarchical design, the upper-level agent supplements the information unavailable to the lower-level agents and provides guidance signals for more coherent decision making.

As shown in Figure 5, lower-level agents 1 and 2 receive as input the masked logarithmic return matrices $\mathbf{q}_{t-1}^{(1)}$ and $\mathbf{q}_{t-1}^{(2)}$, corresponding to the high-quality asset group and the ordinary asset group, respectively. Both agents share an identical network architecture, with differences arising solely from the masks $\mathbf{m}_{t-1}^{(1)}$ and $\mathbf{m}_{t-1}^{(2)}$, which define the effective input domain by filtering out irrelevant assets and thereby reducing the dimensionality of the allocation space [Shen and Shafiq \(2020\)](#). The network consists of three main components:

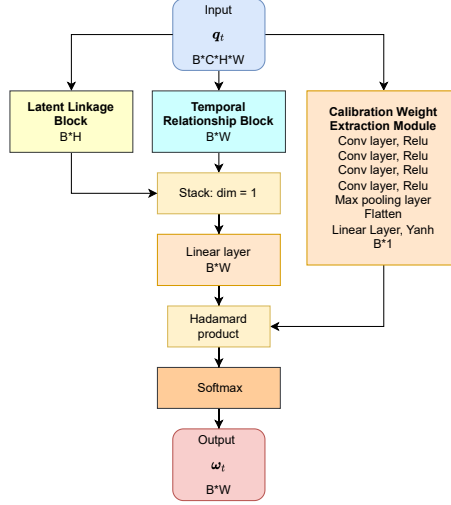


Fig. 4 [Overall workflow of the proposed framework.] Overall workflow of the proposed hierarchical reinforcement learning framework Ren et al. (2025). The framework consists of an upper-level agent, two lower-level agents, and an environment module. The upper-level agent captures global market information and generates coordination signals, which guide the lower-level agents in asset-specific allocation. Each lower-level agent focuses on a distinct subset of assets, extracting local temporal patterns and making portfolio decisions accordingly. The environment provides market observations and reward feedback to complete the learning loop. Detailed descriptions of the module composition and implementation are available in the original work Ren et al. (2025).

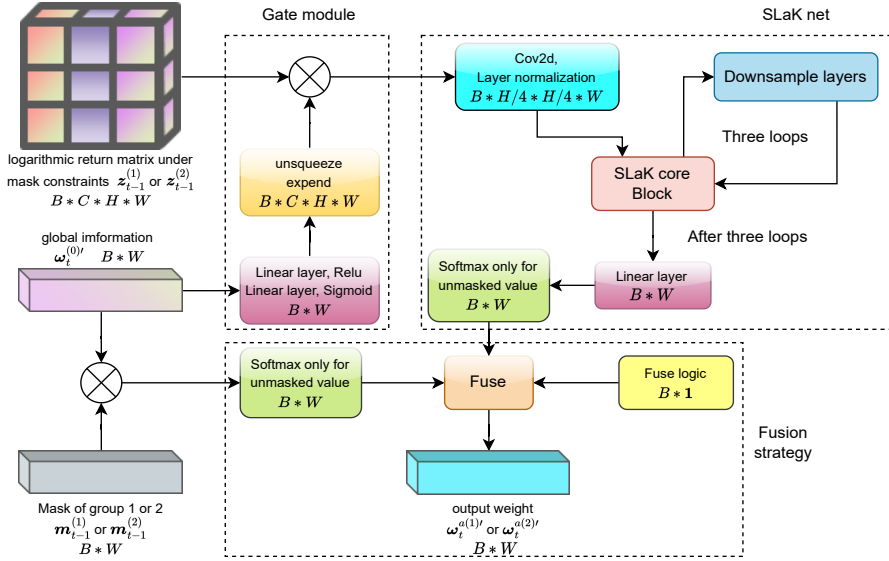


Fig. 5 [Architecture of the lower-level actor network.] Architecture of the lower-level actor network. The network integrates masked logarithmic return matrices, global information from the upper-level agent, and a SLaK backbone to generate intra-group weight distributions, which are subsequently fused with prior signals to obtain group-wise portfolio weights.

1. **Global information integration (Gate module).** The global signal $\omega_t^{(0) \prime}$ produced by the upper-level agent is first transformed through nonlinear mappings to generate gating coefficients. These coefficients perform element-wise multiplication with the input matrices, allowing the lower-level agents to incorporate global market guidance in their intra-group allocation and avoid relying solely on local patterns.

2. **Sparse Large Kernel Network (SLaK) backbone.** The gated return matrix is processed by a SLaK convolutional backbone adopted from [Liu et al. \(2022\)](#). SLaK employs sparsity-enabled kernels with receptive fields extending beyond 51×51 , allowing the network to jointly model temporal dependencies and intra-group correlations. This design substantially enhances representational capacity while preserving computational tractability. The resulting logits are linearly projected and combined with the group masks $\mathbf{m}_{t-1}^{(1)}$ and $\mathbf{m}_{t-1}^{(2)}$ to filter valid entries, followed by a softmax operation that produces the intra-group weight distributions $\omega_t^{(1) \prime}$ and $\omega_t^{(2) \prime}$

3. **Fusion strategy within lower-level agents.** The softmax-based intra-group weights are further combined with the upper-level guidance signal. Specifically, the masked and normalized output of the upper-level agent is computed as

$$\tilde{\omega}_t^{(0) \prime} = \text{softmax}(\omega_t^{(0) \prime} \odot \mathbf{m}_i^{t-1}), \quad i \in \{1, 2\},$$

which represents a group-wise prior distribution. This prior is integrated with the intra-group predictions $\omega_t^{(i) \prime}$, where $i \in \{1, 2\}$, through a convex combination [Vaswani et al. \(2017\)](#), that is, a linear combination with non-negative coefficients summing to one. The combination ratio is controlled by a learnable coefficient λ , constrained to $(0, 1)$ via a sigmoid function, thereby enabling adaptive adjustment between reliance on prior knowledge and data-driven predictions. The fused intra-group allocation is expressed as:

$$\omega_t^{a(i) \prime} = (1 - \lambda) \tilde{\omega}_t^{(0) \prime} + \lambda \omega_t^{(i) \prime}, \quad i \in \{1, 2\}.$$

This design provides several benefits:

- **Consistency of information:** The fusion mechanism ensures coherent coordination between global and local decision modules [Barto and Mahadevan \(2003c\)](#).
- **Finer allocation granularity:** The design preserves the detailed representation power of intra-group modeling while embedding global constraints [Yang et al. \(2020a\)](#).
- **Enhanced interpretability:** The final outputs can be decomposed into global guidance and local optimization, offering transparent insights into the decision process [De Asis et al. \(2018\)](#).

It should be emphasized that the outputs $\omega_t^{(1) \prime}$ and $\omega_t^{(2) \prime}$ represent only relative intra-group weights. The final portfolio weights are determined in the subsequent capital allocation and cross-group fusion mechanism.

The lower-level critic network adopts a transformer-based architecture for value estimation as introduced in [Ren et al. \(2025\)](#). In this setting, the critic encodes state-action pairs and learns the corresponding value function, thereby providing optimization signals for actor updates. The principal modification lies in the incorporation

of masking constraints at the input stage. Specifically, for each group $i \in \{1, 2\}$, the state $\mathbf{z}_{t-1}^{(i)}$ and the action $\boldsymbol{\omega}_t^{(i) \prime}$ are element-wise multiplied with the corresponding mask $\mathbf{m}_{t-1}^{(i)}$ before being fed into the critic, ensuring that value estimation remains confined to the designated asset subset. This design prevents cross-group interference and preserves group-specific independence. Two advantages arise from this modification. First, it maintains coherence with the hierarchical framework, in which the upper-level agent extracts global signals while the lower-level critic performs localized value assessment [Barto and Mahadevan \(2003c\)](#). Second, it enforces consistency between value estimation and dynamic classification, thereby reinforcing the logical closure of the hierarchical decision process [Yang et al. \(2020a\)](#).

4.6 Capital Allocation and Final Portfolio Weights via Utility Optimization

After obtaining the intra-agent weights $\boldsymbol{\omega}_t^{a(1) \prime}$ and $\boldsymbol{\omega}_t^{a(2) \prime}$, we integrate them with classical portfolio selection techniques to determine the allocation of investment capital among the risk-free asset, Group 1, and Group 2. Within the domain of portfolio theory, the mean–variance framework represents one of the most influential and widely applied methodologies. Subsequent developments extend this paradigm by formulating portfolio selection as the maximization of an expected utility function, a perspective that generalizes the trade-off between risk and return. When the utility function is quadratic, the problem of maximizing expected utility can be equivalently expressed as minimizing portfolio variance while maximizing expected return, as discussed in [Bodnar et al. \(2015a\)](#).

In this formulation, the investor seeks to optimize the expected utility of terminal wealth, with preferences encoded through a chosen utility function [Çanakoğlu and Özekici \(2009\)](#). Standard measures of risk aversion are well established in the literature [Pratt \(1978\)](#); [Arrow \(1996\)](#), providing formal foundations for modeling investor behavior. Moreover, [Bertsekas et al. \(2011\)](#) analyzes a class of utility functions and derives optimal multi-period policies under dynamic settings. Leveraging these theoretical foundations, section 4.6 formulates an exponential utility framework to represent investor preferences and derive optimal allocations among the risk-free asset, Group 1, and Group 2.

4.6.1 Maximization of expected utility function

Prior to addressing the primary problem, it is essential to establish some notational conventions. At the commencement of period t , an investor possessing an endowment represented by W_t is tasked with determining the optimal portfolio weights $\boldsymbol{\omega}_t'$ to allocate towards risky assets. This allocation is aimed at maximizing the expected utility of their wealth in the subsequent period, while investing the remainder, represented by $1 - \sum \boldsymbol{\omega}_t'$, in a risk-free asset. The wealth function of these assets can be articulated as follows:

$$W_t = W_{t-1}(1 + r_A) + W_{t-1} [\boldsymbol{\omega}_t'^\top (R_t - \mathbf{1}r_A)] .$$

This formulation encompasses both the risk-free rate and the adjustments for risky asset returns, thereby facilitating a comprehensive analysis of wealth dynamics in the investment strategy. Therefore, the portfolio selection problem is

$$\max_{\omega'_t} \mathbb{E}[U(W_t)].$$

In many instances, obtaining an analytical solution to the expected utility maximization problem is notably challenging, prompting numerous scholars to depend on numerical methods, as referenced in [Brandt and Santa-Clara \(2006\)](#) and [Çanakoğlu and Özekici \(2009\)](#). Nevertheless, a significant number of researchers have successfully derived analytical solutions for various scenarios of the expected utility maximization problem, particularly when the utility function is exponential, as indicated in [Bodnar et al. \(2015b\)](#) and [Rásónyi and Sayit \(2025\)](#).

In the subsequent section, we will articulate the primary contributions derived from our research. In this study, we do not investigate the relationship between optimal portfolio weights and wealth. Consequently, we set the wealth level at $W_t = 1$. Our utility function is expressed as follows:

$$U(x) = -e^{-\alpha x} \quad \alpha > 0.$$

Assuming that the log-return conforms to a Normal distribution, it follows that the expression $R_t - \mathbf{1}r_A$ also follows to a Normal distribution. As a result, the wealth function can be redefined as follows:

$$W_t \stackrel{d}{=} W_{t-1}(1 + r_A) + W_{t-1} \left[\omega_t'^\top (\mu - \mathbf{1}r_A) + \sqrt{\omega_t'^\top \Sigma \omega_t'} N_{(0,1)} \right],$$

where μ represents the expected value of log-returns (at the period t), Σ denotes the covariance of log-returns (at the period t), and $N_{(0,1)}$ is interpreted as the standard normal distribution. Therefore, the expectation of the exponential utility function can be derived as follows:

$$\begin{aligned} \mathbb{E}[U(W_t)] &= -e^{-\alpha W_{t-1}(1+r_A)} e^{-\alpha W_{t-1}[\omega_t'^\top (\mu - \mathbf{1}r_A)]} \\ &\times \int_{-\infty}^{+\infty} e^{-\alpha W_{t-1} \sqrt{\omega_t'^\top \Sigma \omega_t'} x} \varphi(x) dx, \end{aligned}$$

where $\varphi(x)$ denotes the density function of the standard normal distribution.

4.6.2 Optimal solution of maximization

To reformulate the expected exponential utility function, we shall utilize the Fourier transform, as illustrated in the following expression:

$$\max_{\omega'_t} -e^{-\alpha W_{t-1}(1+r_A)} e^{\frac{\alpha^2 W_{t-1}^2}{2} \omega_t'^\top \Sigma \omega_t' - \alpha W_{t-1}[\omega_t'^\top (\mu - \mathbf{1}r_A)]}.$$

Given that $\alpha > 0$, the constant term in the aforementioned objective function is negative, which indicates that the function is decreasing. Therefore, this optimization problem can be reformulated as a quadratic programming problem:

$$\begin{aligned} \min_{\omega'_t \in \mathbb{R}^d} \quad & \frac{\alpha^2 W_{t-1}^2}{2} \omega'^\top \Sigma \omega'_t, \\ \text{s.t.} \quad & \omega'^\top (\mu - \mathbf{1} r_A) = -c. \end{aligned}$$

It is important to note that the initial problem presents significant challenges for analytical resolution. Furthermore, when the dimensionality of the stock variables is exceedingly high, obtaining a numerical solution becomes exceptionally arduous. In this context, we define a hyperplane characterized by the equation $\omega'^\top (\mu - \mathbf{1} r_A) = -c$. Achieving the optimal solution situated below this hyperplane demonstrates enhanced efficiency. Additionally, it is feasible to modify the value of c in response to fluctuating market conditions. This adjustment enables the repositioning of the hyperplane, facilitating the identification of the optimal solution in relation to it.

The solution of this problem can be derived using the Lagrangian method [Jin et al. \(2008\)](#). Accordingly, the Lagrangian function is defined as follows:

$$\mathcal{L}(\omega_t) := \frac{\alpha^2 W_{t-1}^2}{2} \omega'^\top \Sigma \omega'_t - \lambda (\omega'^\top (\mu - \mathbf{1} r_A) + c),$$

where λ denotes the Lagrangian multiplier. By applying the first-order conditions (FOC), one arrives at a system of equations articulated as follows:

$$\begin{cases} \frac{\partial \mathcal{L}}{\partial \omega'_t} = \alpha^2 W_{t-1}^2 \Sigma \omega_t - \lambda (\mu - \mathbf{1} r_A) = 0 \\ \frac{\partial \mathcal{L}}{\partial \lambda} = -\omega'^\top (\mu - \mathbf{1} r_A) - c = 0. \end{cases}$$

In analyzing the system of equations for a specified constant c , we denote the resultant solution as $\omega_t'^c$, which can be expressed in the following manner:

$$\omega_t'^c := -\frac{c}{B} \odot \mathbf{A}.$$

where $B = (\mu - \mathbf{1} r_A)^\top \Sigma^{-1} (\mu - \mathbf{1} r_A)$ and $\mathbf{A} = \Sigma^{-1} (\mu - \mathbf{1} r_A)$. From the analysis presented above, it can be observed that an increase in the parameter c results in a decrease in the allocation to risky assets, denoted as $\omega_t'^c$. This indicates that c serves as a lever to manage investment exposure to risk. Consequently, in a bearish market environment, it is advisable to decrease the value of c . Conversely, during a bullish market, increasing the value of c would be advisable.

4.6.3 Momentum-based Adjustment

To capture the momentum of the recent market, we implement a momentum strength parameter [Moskowitz et al. \(2012\)](#). Initially, we utilize the log-returns from three

distinct periods as the foundation for assessing momentum strength. We define momentum strength as the L^2 norm of the mean log-returns for these periods. Consequently, we introduce a new parameter denoted as β , represented mathematically as follows:

$$\beta = Clip(3\bar{R}_{t-3:t}, l, h),$$

where \bar{R} refers to the mean log-returns, l is the lowest value and h is the highest value. The allocation of weights to risky assets is then expressed by the equation:

$$\omega_t'^* = \omega_t'^c \times (1 + (\beta \odot \tanh(\bar{R}_{t-3:t}))).$$

This formulation allows for a structured approach to investment strategy based on identified momentum dynamics.

To complement this momentum-based adjustment, we further incorporate a rebound detection mechanism [Jegadeesh \(1990\)](#). The objective is to distinguish between genuine rebounds following a significant decline and mere technical recoveries that may occur during an ongoing downtrend.

To avoid allocating heavily during temporary technical recoveries in ongoing down-trends, we incorporate a **rebound detection mechanism**. Let $\bar{R}_{t-m:t}$ denote the recent mean log-return for a group of assets. A rebound is identified if two conditions are simultaneously satisfied:

1. **Downtrend condition:** the mean return over the preceding m periods (e.g. $m = 3$) falls below a negative threshold θ_d , representing a sustained decline:

$$\bar{R}_{t-m:t} < \theta_d$$

2. **Rebound condition:** the most recent one or two periods exhibit returns above a positive threshold θ_u :

$$\bar{R}_{t-1} > \theta_u \quad \text{and} \quad \bar{R}_t > \theta_u$$

Binary indicators of rebounds are computed for each asset group:

$$\text{rebound_flags} = [\text{rebound}_0, \text{rebound}_1]$$

These flags act as validation signals for whether the portfolio should consider adjustments beyond the baseline momentum allocation. To integrate multiple sources of portfolio information while maintaining stability, we implement a **selective fusion mechanism**.

The baseline weights $\omega_t'^*$, is integrated with the generated global masked information, denoted $\omega_t^{(0)i}$, specifically for asset groups that exhibit confirmed rebounds. Formally, for each group i , the updated weights are defined as follows:

$$\omega_t^{new(i)*} = \begin{cases} (1 - \eta) \omega_t^{(i)*} + \eta \omega_t^{0(i)*}, & \text{if } \text{rebound_flags}_i = \text{True} \\ \omega_t^{(i)*}, & \text{otherwise} \end{cases}$$

where $\eta \in [0, 1]$ dictates the intensity of the blending process. The agent weights are calculated by selectively masking the relevant assets within each group and aggregating their individual actions:

$$\omega_t^{0(i)\prime} = \sum_j (\omega_{j,t}^{(0)\prime} \cdot m_{j,t}^{(i)}).$$

This targeted fusion ensures that adjustments informed by adaptive models affect asset allocation only when the market exhibits verified rebound behavior. Asset groups without rebound signals remain consistent with the baseline expected-utility maximizing portfolio, thereby maintaining robustness. To incorporate the risk-free asset into the allocation, the unnormalized logits are constructed by concatenating the fixed baseline element with the outputs of the two risky-asset groups as

$$\omega_t^{set\prime} = [0, \omega_t^{new(1)\prime}, \omega_t^{new(2)\prime}],$$

where the first element corresponds to the risk-free asset and is fixed at zero. Setting its logit to zero provides a stable reference baseline in the softmax normalization, reflecting the financial role of the risk-free asset as a benchmark with negligible sensitivity to market conditions. This treatment eliminates redundant parameterization and leverages the shift-invariance property of the softmax function [LeCun et al. \(2015\)](#). Accordingly, the logits of the two risky asset groups, $\omega_t^{new(1)\prime}$ and $\omega_t^{new(2)\prime}$, quantify their relative attractiveness against the risk-free baseline. After applying the softmax transformation,

$$\omega_t^{capital\prime} = \text{softmax}\left(\frac{\omega_t^{set\prime}}{Tep}\right),$$

where $Tep > 0$ denotes a temperature coefficient controlling the sharpness of the allocation distribution [LeCun et al. \(2015\)](#), we obtain normalized weights $\omega_t^{capital(f)\prime}$, $\omega_t^{capital(1)\prime}$, and $\omega_t^{capital(2)\prime}$, which can be interpreted as probabilities of allocating capital across the risk-free asset and the two risky groups. Given the group-level capital proportions $\omega_t^{capital(1)\prime}$ and $\omega_t^{capital(2)\prime}$, together with the intra-group weight vectors $\omega_t^{a(1)\prime}$ and $\omega_t^{a(2)\prime}$, the final transaction-level allocations $\omega_t^{(1)\prime}$ and $\omega_t^{(2)\prime}$ are computed as

$$\omega_t^{(i)\prime} = \omega_t^{a(i)\prime} \omega_t^{capital(i)\prime}, \quad i \in \{1, 2\},$$

thereby integrating intra-group optimization with group-level capital allocation in a financially coherent manner. This design treats the risk-free asset as a *benchmark-relative anchor* [Sharpe \(1964\)](#), ensuring that risky asset allocations are consistently interpreted with respect to a stable financial baseline.

4.7 Loss Function and Exploration Strategy

The optimization of the lower-level framework is based on the DDPG paradigm, augmented with auxiliary components and enhanced exploration mechanisms.

4.7.1 Critic objective.

The critic network is optimized using a temporal-difference (TD) objective [Silver et al. \(2014\)](#), the canonical method in reinforcement learning for estimating value functions through bootstrapping from subsequent rewards. This formulation is derived from

the Bellman equation [Silver et al. \(2014\)](#), which establishes the recursive structure of value estimation. For a transition $(\mathbf{s}_{t-1}, \mathbf{a}_{t-1}, r_t, \mathbf{s}_t)$, the objective is expressed as

$$\mathcal{L}_{\text{critic}} = \mathbb{E} \left[(r_t + \gamma Q_{\theta^-}(\mathbf{s}_t, \pi_{\phi^-}(\mathbf{s}_t)) - Q_{\theta}(\mathbf{s}_{t-1}, \mathbf{a}_{t-1}))^2 \right],$$

where Q_{θ} represents the critic network parameterized by θ , which estimates the expected return of a state-action pair. The policy π_{ϕ} , parameterized by ϕ , denotes the actor network that generates deterministic portfolio-weight actions. The pairs (θ^-, ϕ^-) correspond to the delayed target parameters used to stabilize training by reducing estimation variance and preventing oscillations during learning.

4.7.2 Actor network objective with detached prior alignment.

The actor network is optimized by maximizing the critic's evaluation of its policy outputs, augmented with two auxiliary components: an entropy regularizer and a detached prior-alignment penalty. The overall objective is formulated as

$$\begin{aligned} \mathcal{L}_{\text{actor}} &= -\mathbb{E}_{\mathbf{s}_t} \left[Q_{\theta}(\mathbf{s}_t, \pi_{\phi}(\mathbf{s}_t)) \right] - \beta \mathcal{H}(\pi_{\phi}(\mathbf{s}_t)) + \alpha \mathcal{L}_{\text{imit}}^{\text{det}}, \\ \mathcal{H}(\pi_{\phi}(\mathbf{s}_t)) &= -\sum_k p_k \log p_k, \quad \tilde{\boldsymbol{\omega}}_t^{(0,i)'} = \text{softmax}(\boldsymbol{\omega}_t^{(0)'} \odot \mathbf{m}_{t-1}^{(i)}), \\ \mathcal{L}_{\text{imit}}^{\text{det}} &= \left\| \text{sg}(\boldsymbol{\omega}_t^{(i)'})) - \text{sg}(\tilde{\boldsymbol{\omega}}_t^{(0,i)'}) \right\|_2^2, \quad i \in \{1, 2\}, \end{aligned}$$

where $\mathcal{H}(\cdot)$ denotes the entropy of the action distribution, $\alpha = 0.1$ and $\beta = 0.01$ are fixed coefficients, and $\text{sg}(\cdot)$ indicates the stop-gradient operator. Because both terms in $\mathcal{L}_{\text{imit}}^{\text{det}}$ are detached, this component introduces no gradient contributions to network parameters and therefore acts as a constant offset in optimization. Its function is to provide a stable diagnostic of the alignment between intra-group predictions $\boldsymbol{\omega}_t^{(i)'}$ and the masked upper-level prior $\tilde{\boldsymbol{\omega}}_t^{(0,i)'}$, while strictly preventing cross-layer gradient propagation [Silver et al. \(2014\)](#).

4.7.3 Exploration mechanism.

To ensure effective exploration in the continuous, high-dimensional action space, the framework employs a hybrid exploration scheme comprising:

- **Ornstein–Uhlenbeck (OU) process noise.** Correlated Gaussian perturbations generated by an OU process are added to the actions, producing temporally coherent trajectories that better capture trading dynamics [Lillicrap et al. \(2015b\)](#).
- **ϵ -greedy perturbation.** With probability ϵ , the action is perturbed by zero-mean Gaussian noise and subsequently clipped to admissible bounds, thereby injecting stochasticity and mitigating entrapment in local optima [Sutton and Barto \(1998\)](#).

Together, these components balance exploration and exploitation: OU-process noise promotes stability and temporal smoothness, whereas ϵ -greedy perturbations enhance resilience in volatile market conditions.

5 Experiment

5.1 Data

We construct three independent datasets from Yahoo Finance¹, with the Dow Jones Industrial Average (DJIA) serving as the empirical foundation of the analysis. The DJIA is selected as the benchmark for the SAMP-HDRL framework because it comprises 30 highly liquid equities from diverse industries, thereby providing a representative market environment consistent with the assumptions of this study. Each dataset spans a four-year horizon, in which the first three years function as the training set and the final year is reserved for backtest, as summarized in Table 3. To evaluate the robustness of SAMP-HDRL under extreme market turbulence induced by exogenous shocks, particular emphasis is placed on the backtest set of Dataset 2 and the training set of Dataset 3, especially those reflecting the pronounced volatility observed during the COVID-19 pandemic in 2020 [Apergis et al. \(2023\)](#).

While reinforcement learning provides adaptive mechanisms for sequential decision-making, it cannot fully resolve the challenges posed by non-stationary market dynamics. Hence, before evaluating model performance, it is necessary to characterize the statistical properties of the datasets, particularly the 2020 segment where the COVID-19 pandemic triggered circuit breakers and induced structural breaks in U.S. equity markets. For this purpose, we apply two standard diagnostic tests to the DJIA. As reported in Table 2, the Augmented Dickey–Fuller (ADF) test [SAID and DICKEY \(1984\)](#) fails to reject the unit-root null hypothesis, confirming that the price series is non-stationary, whereas the ARCH–LM test [Patilea and Raïssi \(2014\)](#) strongly rejects the null hypothesis of homoscedasticity, indicating pronounced conditional heteroscedasticity and volatility clustering in the return sequence. Taken together, these findings confirm that the 2020 market exhibits both non-stationarity and time-varying volatility, consistent with the exceptional turbulence of that year. Alongside the upward-trending regime in 2019 [Kyriazis et al. \(2023\)](#); [Wang et al. \(2021\)](#) and the oscillatory dynamics of 2021 [Ullah et al. \(2023\)](#), these diagnostics establish a rigorous basis for evaluating SAMP-HDRL under heterogeneous environments, thereby enabling a comprehensive assessment of robustness and adaptability. Because Dow Inc. was separated from DowDuPont in March 2019, consistent histori-

Table 2 Unit root and conditional heteroscedasticity tests for DJIA in 2020

Test	Statistic	p-value
ADF (Price series)	−1.7258	0.4179
ARCH–LM (Return series)	99.0891	$< 1 \times 10^{-16}$

cal records before March 18, 2019, are unavailable [INSIDER \(2023\)](#). Accordingly, this

¹ <http://www.finance.yahoo.com>

stock is excluded from the analysis, leaving 29 constituents in the sample. The trading horizon is defined on a daily scale, and the adjusted closing price of each equity is employed to construct the price matrix. Compared with raw closing prices, adjusted closing prices correct for distortions arising from dividends and stock splits [Gao and Chai \(2018\)](#), thereby providing a more accurate, comparable, and methodologically coherent representation of asset values [Huang \(2024\)](#).

Table 3 Data Range for training datasets and backtest datasets

Data Purpose	Training Data Range	Backtest Data Range
Backtest 1	2016/01/01 00:00 to 2019/01/01 00:00	2019/01/01 00:00 to 2020/01/01 00:00
Backtest 2	2017/01/01 00:00 to 2020/01/01 00:00	2020/01/01 00:00 to 2021/01/01 00:00
Backtest 3	2018/01/01 00:00 to 2021/01/01 00:00	2021/01/01 00:00 to 2022/01/01 00:00

5.2 Comparison strategy

We benchmark our framework against nine traditional strategies and nine reinforcement learning (RL)-based approaches, three of which are obtained from the TradeMaster platform [Sun et al. \(2023\)](#). The deep reinforcement learning (DRL) baselines include Ensemble of Identical Independent Evaluators (EIIE) [Jiang et al. \(2017\)](#), FinRL [Liu et al. \(2020\)](#), Ensemble Stock Transactions (EST) [Yang et al. \(2020b\)](#), State-Augmented RL (SARL) [Sun et al. \(2023\)](#), Investor-Imitator (II) [Sun et al. \(2023\)](#), TradeMaster (PPO) [Sun et al. \(2023\)](#), the portfolio policy network with cost sensitivity (PPN) [Zhang et al. \(2020\)](#), TARN [Zhao et al. \(2023\)](#), Deep Modern Portfolio Theory (DeepMPT) [Jang and Seong \(2023\)](#), LSRE-CAAN [Li et al. \(2023\)](#), and Financial Transformer Reinforcement Learning (FTRL) [Ren et al. \(2025\)](#). This collection spans widely adopted DRL benchmarks as well as recent approaches that have gained academic visibility, ensuring both methodological breadth and relevance for comparison.

EIIE introduces a DRL framework originally applied to cryptocurrency portfolios and demonstrates superior performance relative to heuristic strategies; this design is extended to the stock domain as a comparator against SAMP-HDRL. FinRL provides a standardized platform for automated trading, offering unified data preprocessing, environment construction, and training pipelines, thereby ensuring consistency and reproducibility. EST ensembles A2C, DDPG, and PPO to exploit their complementary strengths, representing a multi-algorithm baseline. SARL fuses heterogeneous data sources to capture high-dimensional features and improve robustness, while II encodes trading expertise within a DRL paradigm, enhancing performance across diverse metrics. TradeMaster (PPO) applies automated machine learning for adaptive hyperparameter selection within PPO. PPN emphasizes latent inter-asset dependencies and introduces a cost-sensitive reward to strengthen risk control, whereas TARN explicitly models inter-asset correlations to balance risk and return under dynamic conditions. Two recent approaches that have attracted significant academic attention since 2023 are also considered. DeepMPT integrates Modern Portfolio Theory's risk-return principles with DRL optimization, enabling adaptive allocation in

non-stationary environments, while LSRE-CAAN designs efficient representations, action spaces, and reward functions to capture temporal dependencies and market non-stationarity in high-frequency settings. Finally, FTRL employs a Transformer-based architecture to model temporal dependencies and cross-asset interactions, thereby addressing the limitations of conventional time-series models in portfolio optimization and providing a strong benchmark under comparable conditions. Detailed specifications of all baselines are summarized in Table 4.

To ensure fairness and computational consistency across all baselines, a unified hyperparameter protocol is adopted. A common learning rate is applied across frameworks to ensure consistent training dynamics, taking into account the limited training horizon (755 daily steps), the architectural complexity of Transformer-based models, and the use of automatic mixed precision (AMP) [Micikevicius et al. \(2017\)](#), which stabilizes optimization through reduced gradient magnitudes. Batch size remains fixed for all methods, and a uniform early-stopping criterion is enforced. Architecture-specific hyperparameters, such as the number of layers or attention heads, are not standardized, since these components are absent in certain baselines (e.g., traditional heuristics or simpler DRL models). To prevent bias from extensive hyperparameter tuning and to guarantee reproducibility, exhaustive grid search is deliberately avoided [Henderson et al. \(2018\)](#). Instead, a restricted set of widely adopted values is manually validated and consistently applied throughout the experimental setting.

Table 4 The comparison strategies and their classification

Benchmarks	Uniform Constant Rebalanced Portfolios (CRP) Kelly (1956) Uniform Buy And Hold (UBAH) Cover (1991) Markov of order zero (M0) Li and Hoi (2014)
Follower-the-Winner	Universal Portfolios (UP) Borodin et al. (2000) Exponential Gradient (EG) Hempel et al. (1998)
Follower-the-Lose	Passive Aggressive Mean Reversion (PAMR) Li et al. (2012) Confidence Weighted Mean Reversion (CWMR) Li et al. (2011b)
Pattern-Marching	Correlation-driven Nonparametric Learning Strategy (CORN) Li et al. (2011a)
Financial Theory	Capital Asset Pricing Model (CAPM) Sharpe (1964)
Reinforcement learning strategies	EIE Jiang et al. (2017) Finrl Liu et al. (2020) EST Yang et al. (2020b) SARL Sun et al. (2023) II Sun et al. (2023) PPO Sun et al. (2023) PPN Zhang et al. (2020) TARN Zhao et al. (2023) DeepMPT Jang and Seong (2023) LSRE-CAAN Li et al. (2023) FTRL Ren et al. (2025)

5.3 Performance Measures

The evaluation of the proposed framework is conducted along two primary dimensions: profitability and risk. Profitability is measured by the final cumulative return R_f ,

defined as

$$R_f = \sum_{t=1}^F \varphi_t,$$

where φ_t denotes the portfolio return at time t . A larger R_f reflects stronger overall profitability across the backtest horizon. Risk assessment employs three well-established metrics: the Sharpe ratio r_{Sharpe} [Sharpe \(1998\)](#), the Sortino ratio r_{Sortino} [Rollinger and Hoffman \(2013\)](#), and the Omega ratio r_{Omega} [Keating and Shadwick \(2002\)](#). The Sharpe ratio quantifies excess return relative to total volatility:

$$r_{\text{Sharpe}} = \frac{\mathbb{E}[\varphi_t - r_A]}{\sqrt{\text{Var}(\varphi_t)}},$$

where \mathbb{E} and Var denote the expectation and variance operators, and r_A is the daily log risk-free rate. Recognizing that upward price fluctuations should not be classified as risk [Rollinger and Hoffman \(2013\)](#), the Sortino ratio isolates downside volatility:

$$r_{\text{Sortino}} = \frac{\mathbb{E}[\varphi_t - r_A]}{\sqrt{\frac{1}{j} \sum_{\varphi_t < r_A}^j (\varphi_t - r_A)^2}},$$

where r_A is the minimum acceptable return (set to r_A in this study), and j is the number of periods with $\varphi_t < r_A$. A higher r_{Sortino} reflects superior performance relative to downside risk. The Omega ratio evaluates the entire distribution of returns, incorporating higher-order moments:

$$r_{\text{Omega}} = \frac{\sum_{\varphi_t \geq r_A}^j (\varphi_t - r_A)}{\sum_{\varphi_t < r_A}^j (r_A - \varphi_t)},$$

with r_A again denoting the minimum acceptable return. A larger r_{Omega} indicates stronger dominance of gains over losses, thus providing a more comprehensive characterization of portfolio quality.

5.4 Results and Discussion

We obtained the results in Tables 5 to 7 by conducting experiments on data sets. Daily cumulative returns of strategies are given in Figures 6 to 8. In Backtest 1, SAMP-HDRL outperforms all strategies except FTRL, achieving at least 74%, 34%, 52%, and 13% higher values in Return, Sharpe Ratio, Sortino Ratio, and Omega Ratio, respectively. In Backtest 2, SAMP-HDRL demonstrates clear superiority over all strategies, with improvements of at least 33%, 34%, 36%, and 5% across the four metrics. In Backtest 3, SAMP-HDRL still maintains an advantage, exceeding all other methods by at least 5%, 5%, 5%, and 2% in Return, Sharpe Ratio, Sortino Ratio, and Omega Ratio, respectively.

It is noteworthy that the time period corresponding to Backtest 1 represents a relatively stable and upward-trending market environment [Kyriazis et al. \(2023\)](#);

Table 5 Backtest 1, performance comparison across strategies (best values in each column are highlighted in bold).

Strategy	Return	Sharpe Ratio	Sortino Ratio	Omega Ratio
SAMP-HDRL	0.5652	0.1720	0.1580	1.6025
CRP	0.3251	0.1277	0.1043	1.4194
UBAH	0.3226	0.1274	0.1050	1.4180
M0	0.3152	0.1122	0.0926	1.3600
UP	0.3250	0.1278	0.1044	1.4196
EG	0.3175	0.1233	0.1031	1.4005
PAMR	-0.5208	-0.0930	-0.0834	0.7708
CWMR	-0.5307	-0.0924	-0.0828	0.7735
CORNK	-0.1476	-0.0407	-0.0452	0.8960
CAPM	-0.5079	-0.1618	-0.1620	0.6447
EIIE	0.3112	0.1213	0.1010	1.4026
FinRL	0.1380	0.0215	0.0156	1.0813
EST	0.2384	0.0987	0.0881	1.3334
II	0.0878	0.0175	0.0102	1.0499
SARL	0.2299	0.0911	0.0712	1.2841
PPO	0.2893	0.1103	0.0907	1.3619
PNN	0.0062	0.0014	-0.0059	1.0040
DPG	0.1617	0.0382	0.0300	1.1057
TARN	0.3195	0.1256	0.1032	1.4118
DeepMPT	0.2349	0.0519	0.0422	1.1680
LSRE-CAAN	0.3169	0.1242	0.1033	1.4041
FTRL	0.6722	0.1829	0.2379	1.6523

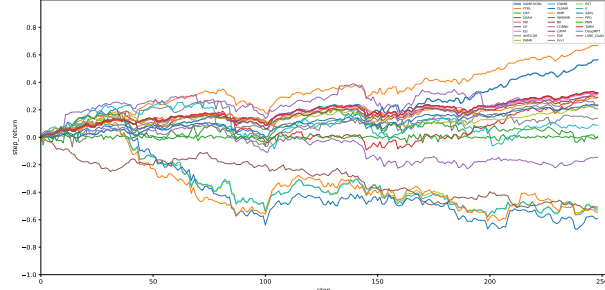


Fig. 6 Daily cumulative return rate for Backtest 1. It depicts the volatility of FTRL cumulative returns and the comparative strategy in Backtest 1.

Wang et al. (2021). Within this setting, SAMP-HDRL underperforms FTRL by approximately 16%, highlighting the sensitivity of the proposed framework to persistently bullish market regimes. This observation can be attributed to two key factors. First, FTRL does not incorporate explicit risk management, thereby allowing the strategy to fully exploit upward trends and maximize profitability in such conditions Ren et al. (2025). Second, the hierarchical architecture of SAMP-HDRL

Table 6 Backtest 2, performance comparison across strategies (best values in each column are highlighted in bold).

Strategy	Return	Sharpe Ratio	Sortino Ratio	Omega Ratio
SAMP-HDRL	0.7047	0.0816	0.0712	1.2744
CRP	0.1591	0.0196	0.0145	1.0659
UBAH	0.0990	0.0121	0.0076	1.0402
M0	0.1669	0.0202	0.0154	1.0667
UP	0.1580	0.0195	0.0144	1.0655
EG	0.0936	0.0121	0.0073	1.0402
PAMR	-1.3773	-0.0996	-0.0882	0.7020
CWMR	-1.3641	-0.0986	-0.0874	0.7047
CORNK	-0.6349	-0.0595	-0.0633	0.8413
CAPM	-0.7527	-0.1299	-0.1181	0.6504
EIIE	0.1261	0.0165	0.0116	1.0553
FinRL	0.0817	0.0048	0.0029	1.0178
EST	0.0111	0.0026	-0.0040	1.0075
II	0.4620	0.0460	0.0431	1.1424
SARL	0.0336	0.0040	0.0005	1.0128
PPO	0.0994	0.0126	0.0081	1.0419
PNN	-0.0094	-0.0005	-0.0022	0.9983
DPG	-0.2163	-0.0152	-0.0169	0.9528
TARN	0.1553	0.0190	0.0140	1.0640
DeepMPT	-0.0728	-0.0059	-0.0078	0.9819
LSRE-CAAN	0.1897	0.0231	0.0177	1.0780
FTRL	0.5292	0.0606	0.0519	1.2059

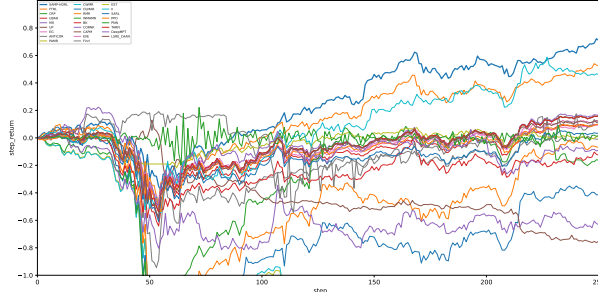


Fig. 7 Daily cumulative return rate for Backtest 2. It depicts the volatility of FTRL cumulative returns and the comparative strategy in Backtest 2.

not only captures temporal patterns but also integrates structural mechanisms for risk balancing and robustness [Barto and Mahadevan \(2003b\)](#). This design creates a dynamic trade-off between return maximization and risk control. Under relatively calm and upward-trending conditions, this trade-off may suppress certain high-risk, high-reward opportunities, resulting in marginally lower returns compared to the

Table 7 Backtest 3, performance comparison across strategies (best values in each column are highlighted in bold).

Strategy	Return	Sharpe Ratio	Sortino Ratio	Omega Ratio
SAMP-HDRL	0.3938	0.1101	0.1004	1.3328
CRP	0.2795	0.1032	0.0899	1.3129
UBAH	0.2798	0.1023	0.0889	1.3092
M0	0.2255	0.0721	0.0606	1.2059
UP	0.2788	0.1030	0.0899	1.3121
EG	0.2612	0.0931	0.0788	1.2799
PAMR	-0.7418	-0.1372	-0.1340	0.6862
CWMR	-0.7830	-0.1403	-0.1383	0.6793
CORNK	-0.4646	-0.0909	-0.0868	0.7682
CAPM	-0.4190	-0.1209	-0.1215	0.6997
EIIE	0.2269	0.0880	0.0736	1.2625
FinRL	0.2018	0.0252	0.0177	1.1093
EST	0.1626	0.0525	0.0416	1.1463
II	0.1828	0.0455	0.0371	1.1286
SARL	0.1607	0.0520	0.0408	1.1425
PPO	0.2253	0.0860	0.0729	1.2543
PNN	0.0034	0.0008	-0.0064	1.0020
DPG	0.1337	0.0253	0.0218	1.0700
TARN	0.2798	0.1029	0.0894	1.3130
DeepMPT	0.0451	0.0079	0.0024	1.0248
LSRE-CAAN	0.2813	0.1025	0.0892	1.3121
FTRL	0.3746	0.1048	0.0949	1.3070

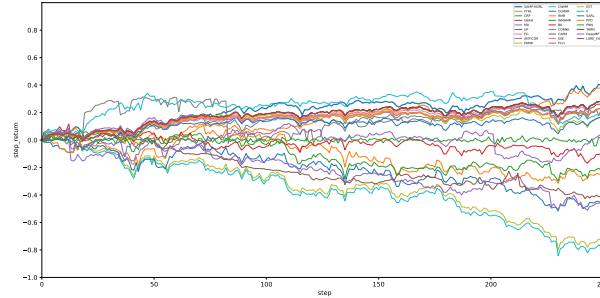


Fig. 8 Daily cumulative return rate for Backtest 3. It depicts the volatility of FTRL cumulative returns and the comparative strategy in Backtest 3.

purely return-oriented FTRL [Driessens et al. \(2019\)](#); [Xiong et al. \(2022\)](#). Nevertheless, when market volatility intensifies or uncertainty becomes dominant [Apergis et al. \(2023\)](#), this mechanism is more advantageous, as evidenced by the superior performance of SAMP-HDRL in Backtest 2.

Table 8 Comparison of FTRL, FTRL-risk, and SAMP-HDRL across three backtest datasets (best values in each column are highlighted in bold).

Backtest	Strategy	Return	Sharpe Ratio	Sortino Ratio	Omega Ratio
Backtest 1	FTRL-risk	0.5167	0.1572	0.1454	1.5402
	FTRL	0.6722	0.1829	0.2379	1.6523
	SAMP-HDRL	0.5652	0.1720	0.1580	1.6025
Backtest 2	FTRL-risk	0.6866	0.0794	0.0710	1.2672
	FTRL	0.5292	0.0606	0.0519	1.2059
	SAMP-HDRL	0.7047	0.0816	0.0712	1.2744
Backtest 3	FTRL-risk	0.3916	0.1095	0.0970	1.3316
	FTRL	0.3746	0.1048	0.0949	1.3070
	SAMP-HDRL	0.3938	0.1101	0.1004	1.3328

To further validate the findings, an additional set of experiments is conducted with a variant of FTRL, denoted as FTRL-risk. This extension augments the original FTRL by incorporating a lower-level module for dynamic asset classification and capital allocation, consistent with the design of SAMP-HDRL. The three backtest datasets are used, and the results are summarized in Table 8, which reports the performance of FTRL, its risk-augmented variant, and SAMP-HDRL. In the time period corresponding to Backtest 1, characterized by a relatively stable and upward-trending market, FTRL achieves the best outcomes across all metrics, surpassing SAMP-HDRL by 19%, 6%, 51%, and 3% in Return, Sharpe ratio, Sortino ratio, and Omega ratio, respectively. By contrast, FTRL-risk underperforms FTRL, with the same metrics being lower by 23%, 14%, 39%, and 7%, respectively, confirming the inference that explicit risk control may suppress high-risk, high-reward opportunities in bullish regimes [Driessen et al. \(2019\)](#); [Xiong et al. \(2022\)](#). In the period corresponding to Backtest 2, marked by heightened volatility [Apergis et al. \(2023\)](#), SAMP-HDRL consistently outperforms all strategies, exceeding FTRL by 33%, 35%, 37%, and 6% in the four metrics, respectively. FTRL-risk also improves upon FTRL with gains of 30%, 31%, 37%, and 5%, respectively, indicating that risk-sensitive modifications enhance profitability and risk-adjusted performance, though still falling short of the robustness achieved by SAMP-HDRL. In the time horizon of Backtest 3, reflecting sideways and mixed conditions [Ullah et al. \(2023\)](#), SAMP-HDRL again maintains the lead, outperforming FTRL by 5%, 5%, 6%, and 2% in Return, Sharpe ratio, Sortino ratio, and Omega ratio, respectively, while FTRL-risk shows modest improvements of 5%, 4%, 2%, and 2% over FTRL, respectively, yet remains inferior to SAMP-HDRL overall. Overall, these results reinforce the prior analysis: while FTRL benefits most in stable upward markets due to the absence of explicit risk constraints, the integration of risk control substantially strengthens resilience in volatile and uncertain environments, enabling SAMP-HDRL to achieve a more effective dynamic balance between return maximization and risk management.

Table 9 Ablation study of SAMP-HDRL, performance comparison with different modules removed across three backtest datasets (best values in each column are highlighted in bold).

Backtest	Strategy	Return	Sharpe Ratio	Sortino Ratio	Omega Ratio
Backtest 1	SAMP-HDRL w/o upper	0.4391	0.1479	0.1306	1.4917
	SAMP-HDRL w/o lower	0.6722	0.1829	0.2379	1.6523
	SAMP-HDRL w/o dc	0.2639	0.1025	0.0820	1.3135
	SAMP-HDRL w/o ca	0.4545	0.1570	0.1370	1.5408
	SAMP-HDRL	0.5652	0.1720	0.1580	1.6025
Backtest 2	SAMP-HDRL w/o upper	0.5103	0.0611	0.0512	1.2110
	SAMP-HDRL w/o lower	0.5292	0.0606	0.0519	1.2059
	SAMP-HDRL w/o dc	0.6284	0.0713	0.0647	1.2363
	SAMP-HDRL w/o ca	0.4679	0.0553	0.0467	1.1897
	SAMP-HDRL	0.7047	0.0816	0.0712	1.2744
Backtest 3	SAMP-HDRL w/o upper	0.3265	0.0977	0.0897	1.2887
	SAMP-HDRL w/o lower	0.3746	0.1048	0.0949	1.3070
	SAMP-HDRL w/o dc	0.3895	0.1118	0.1047	1.3354
	SAMP-HDRL w/o ca	0.3481	0.1099	0.1017	1.3352
	SAMP-HDRL	0.3938	0.1101	0.1004	1.3328

To further validate the effectiveness and necessity of the proposed innovations in SAMP-HDRL—namely upper–lower coordination, dynamic clustering, and capital allocation—we design a set of ablation experiments. Specifically, four variants of SAMP-HDRL are constructed: SAMP-HDRL w/o upper, SAMP-HDRL w/o lower, SAMP-HDRL w/o dc, and SAMP-HDRL w/o ca, which remove the upper-level framework, the lower-level agents, the dynamic clustering module, and the capital allocation module, respectively. To ensure operability, in SAMP-HDRL w/o upper the upper framework is replaced with the UBAH [Cover \(1991\)](#) strategy to provide global decision outputs, thereby testing its contribution to inter-asset correlation modeling. In SAMP-HDRL w/o lower, the entire lower-level agent structure is removed to examine its role in intra-asset temporal modeling and risk control. In SAMP-HDRL w/o dc, the dynamic clustering mechanism is replaced by a static clustering procedure performed before training, verifying its advantage in adapting to evolving market structures. Finally, in SAMP-HDRL w/o ca, the original capital allocation mechanism is replaced by equal allocation between asset groups, in order to assess its contribution to optimizing the risk–return trade-off. The empirical results are reported in Table 9.

Table 9 reports the performance of SAMP-HDRL and its ablated variants across the three backtest datasets. The results demonstrate that the proposed innovations—upper–lower coordination, dynamic clustering, and capital allocation—play indispensable roles in enhancing overall performance.

In the time period corresponding to Backtest 1, SAMP-HDRL outperforms the variant without the upper framework by 29%, 16%, 21%, and 7% in Return, Sharpe ratio, Sortino ratio, and Omega ratio, respectively. Relative to the variant without dynamic clustering, the improvements are 114%, 68%, 93%, and 22%, respectively, while relative to the variant without capital allocation, the gains are 24%, 10%, 15%, and 4%, respectively. However, the variant without the lower agents achieves a Return higher than SAMP-HDRL by 19%, confirming the earlier inference that

risk-control mechanisms may restrict profit maximization under one-sided upward conditions [Driessen et al. \(2019\)](#); [Xiong et al. \(2022\)](#).

In the interval of Backtest 2, characterized by heightened volatility, SAMP-HDRL demonstrates consistent superiority. Compared with the variant without the upper framework, the improvements are 38%, 34%, 39%, and 5% in the four metrics, respectively. Relative to the variant without the lower framework, the gains are 33%, 35%, 37%, and 6%, respectively. Against the variant without dynamic clustering, the improvements are 12%, 14%, 10%, and 3%, respectively, while relative to the variant without capital allocation, the margins rise to 51%, 47%, 53%, and 7%, respectively. These results underscore that all three mechanisms contribute indispensably to robustness and the risk–return balance under turbulent conditions.

In the horizon of Backtest 3, reflecting sideways and mixed market conditions, SAMP-HDRL outperforms the variant without the upper framework by 21%, 13%, 12%, and 3% in Return, Sharpe ratio, Sortino ratio, and Omega ratio, respectively, and exceeds the variant without the lower framework by 5%, 1%, 2%, and 2%, respectively. Relative to the variant without capital allocation, the improvements are 13%, 0.1%, -1% , and -0.2% in the same metrics, respectively. When compared with the variant without dynamic clustering, SAMP-HDRL achieves an increase of 1% in Return but decreases of 2% and 0.3% in Sharpe and Sortino ratios, respectively, while its Omega ratio is slightly lower by 0.2%. This indicates that dynamic clustering is particularly effective in optimizing the risk–return trade-off in non-trending markets.

Overall, the ablation study validates the effectiveness of the three key innovations: the upper framework substantially strengthens robustness through inter-asset correlation modeling, the lower agents are indispensable for risk control in volatile markets, and dynamic clustering together with capital allocation effectively optimize the risk–return balance in structurally shifting and oscillating environments, thereby underpinning the overall superiority of SAMP-HDRL.

SHapley Additive exPlanations (SHAP) [Lundberg and Lee \(2017\)](#) offers a cooperative game–theoretic framework for interpretability by attributing the marginal contribution of each input feature to the model output in a fair manner. In this study, SHAP is integrated into the DRL-based portfolio allocation framework to quantify the influence of each asset’s historical price trajectory on the assigned portfolio weights. Specifically, for each backtest period, SHAP values are computed for the actions of both lower-level agents, capturing how past market movements and clustering masks contribute to allocation decisions.

The resulting visualizations (Figures 9 to 11) consist of three subplots corresponding to distinct market regimes. In each subplot, the vertical axis represents the temporal dimension (trading days), while the horizontal axis corresponds to individual assets. The panels labeled R1–R4 correspond to the four post-reclassification periods in which cluster memberships remain stable, and ALL provides the aggregated view across the full year. The color intensity encodes the SHAP value magnitude, indicating each asset’s contribution to portfolio weight decisions at a given time. Warm colors denote positive contributions that increase allocation weights, whereas cool colors indicate negative contributions leading to reduced exposure. The superimposed

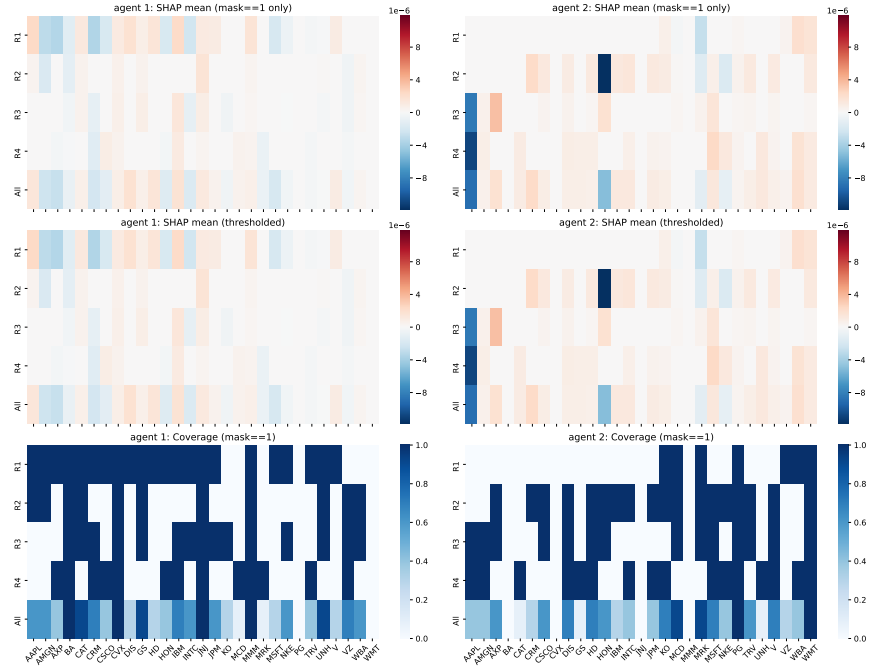


Fig. 9 SHAP analysis 1. SHAP analysis for Backtest 1 (2019), showing mean, thresholded, and coverage visualizations. Agent 1 (remaining assets) provides broad diversification, while Agent 2 (high-quality assets) focuses on core contributors.

trend lines highlight periods of regime transition or allocation shifts, allowing direct visual comparison of agent attention across market phases.

To capture the model's explanatory behavior from multiple perspectives, three complementary SHAP visualizations are presented. The mean SHAP plot reflects the overall magnitude of asset contributions by averaging absolute SHAP values over time, thus revealing globally dominant drivers of portfolio allocation. The thresholded SHAP visualization focuses on periods where SHAP magnitudes exceed a specified significance level, filtering out minor fluctuations and emphasizing decisive yet infrequent allocation impulses. In contrast, the coverage SHAP plot quantifies how frequently each asset exhibits substantial influence, thereby capturing the persistence and stability of its contribution across trading periods. Together, these three visual perspectives jointly describe both the intensity and temporal prevalence of feature impacts, enabling a more comprehensive interpretation of agent decision dynamics.

Examination of these SHAP patterns further reveals that the two lower-level agents exhibit complementary behaviors: Agent 1 maintains wide coverage across assets to ensure diversification, while Agent 2 concentrates on high-quality clusters that dominate returns during key uptrends. The temporal synchronization between these two attention patterns provides empirical evidence that the hierarchical coordination mechanism effectively adapts to varying market regimes, thereby enhancing both interpretability and transparency of the overall DRL decision process.

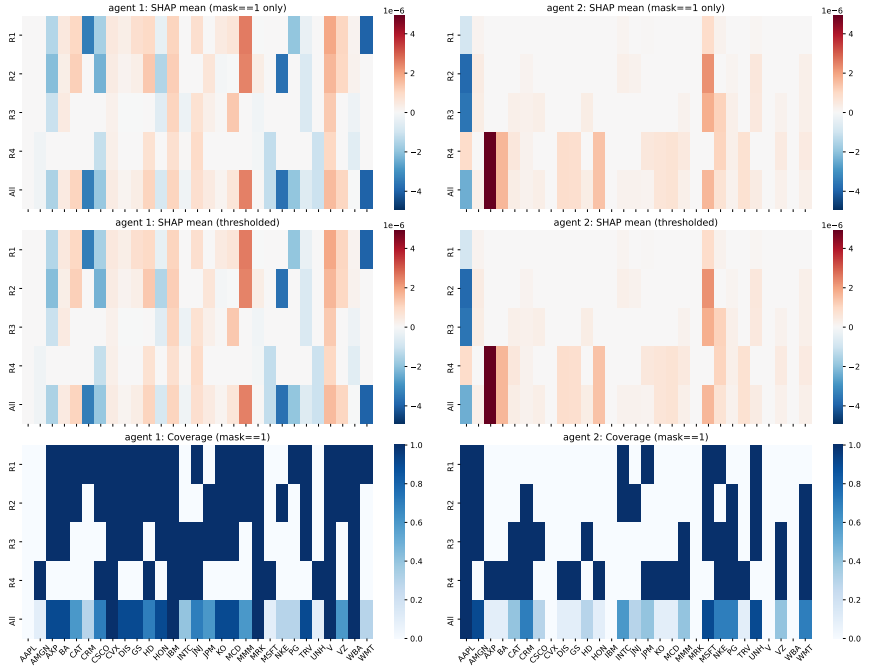


Fig. 10 SHAP analysis 2. SHAP analysis for Backtest 2 (2020), showing mean, thresholded, and coverage visualizations. Agent 1 (remaining assets) provides broad diversification, while Agent 2 (high-quality assets) focuses on core contributors.

Figures 9 to 11 presents the SHAP interpretability results of SAMP-HDRL across Backtest 1 (2019), Backtest 2 (2020), and Backtest 3 (2021), corresponding to a stable upward market, a non-stationary market, and a recovery phase with oscillating dynamics, respectively. Overall, the two lower-level agents exhibit a clear division of roles: Agent 1, which manages the remaining assets, maintains broad coverage to ensure diversification, while Agent 2, which focuses on high-quality assets, allocates concentrated attention to the core drivers of portfolio performance. This “diversified + concentrated” coordination adapts dynamically to varying market regimes, thereby enhancing the interpretability of an otherwise black-box DRL policy.

In the stable upward market of 2019 Kyriazis et al. (2023); Wang et al. (2021), Agent 1 distributes attention broadly across assets to sustain diversification, whereas Agent 2 concentrates on high-quality sectors such as technology and finance. Both the SHAP mean and thresholded analyses highlight the persistent positive contributions of these core assets during key upward phases. This complementary allocation aligns with the market's unidirectional growth, enabling the model to capture structural gains while preserving robustness.

In the non-stationary market of 2020 [Apergis et al. \(2023\)](#), the COVID-19 shock induces abrupt shifts in asset risk exposures. The SHAP mean results reveal frequent switches between positive and negative contributions, reflecting adaptive responses to

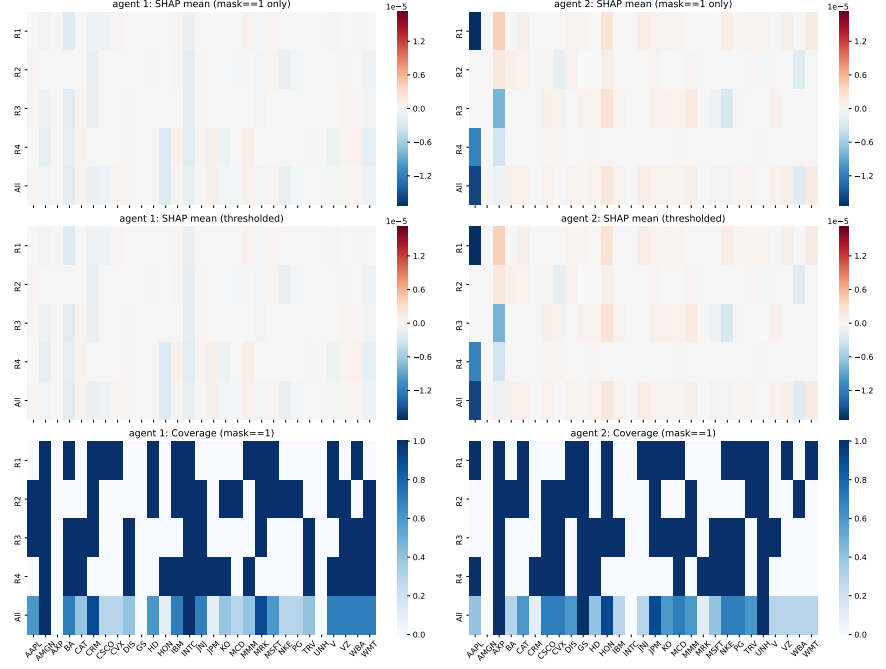


Fig. 11 SHAP analysis 3. SHAP analysis for Backtest 3 (2021), showing mean, thresholded, and coverage visualizations. Agent 1 (remaining assets) provides broad diversification, while Agent 2 (high-quality assets) focuses on core contributors.

heightened uncertainty. Agent 1 continues to maintain broad coverage to buffer systemic risk, while Agent 2 sharply narrows its focus to a small set of high-confidence quality assets, capturing rebounds and structural opportunities. The thresholded SHAP results confirm that the model effectively filters noise in this turbulent environment, retaining only decisive features and thereby demonstrating robustness under non-stationarity.

In the oscillating recovery of 2021 Ullah et al. (2023), the market exhibits upward tendencies accompanied by heightened volatility and uncertainty. The SHAP mean results show relatively smaller marginal contributions across assets, indicating weaker single-stock drivers. Agent 1 maintains balanced coverage across most assets to mitigate risks, whereas Agent 2 selectively emphasizes a few quality assets during specific intervals, forming concentrated allocations. The thresholded SHAP analysis further validates a “broad coverage + selective focus” strategy, balancing risk and return in a sideways environment.

Taken together, the SHAP analyses across three regimes demonstrate that the two lower-level agents do not allocate weights arbitrarily but instead operate through a complementary mechanism. Agent 1 ensures diversification across remaining assets, while Agent 2 concentrates on high-quality assets. This coordination enables the policy to emphasize structural drivers in upward markets, reinforce risk buffering in non-stationary regimes, and integrate diversification with selective focus in oscillating

recoveries. Such behavior not only substantiates the rationality of the agents' decisions but also enhances the interpretability and credibility [Guan and Liu \(2022\)](#) of DRL-based portfolio optimization.

6 Conclusions and Future Plan

This study introduces SAMP-HDRL, a novel hierarchical deep reinforcement learning framework for portfolio management that integrates upper–lower agent coordination, dynamic clustering, and capital allocation. Extensive experiments on three backtest datasets demonstrate that SAMP-HDRL consistently and significantly outperforms both traditional baselines and recent DRL methods across return, Sharpe ratio, Sortino ratio, and Omega ratio. To the best of our knowledge, we are the first to provide a comprehensive integration of hierarchical coordination, clustering, and capital allocation within a unified end-to-end paradigm for portfolio optimization. Comparative and ablation analyses confirm the indispensable contributions of each module: the upper framework enhances inter-asset correlation modeling, the lower agents strengthen risk control, and the combination of clustering with capital allocation ensures an effective balance between diversification and focused allocation. Moreover, SHAP-based interpretability analysis reveals that the two lower-level agents operate in a complementary manner, with Agent 1 supporting diversification across remaining assets and Agent 2 concentrating on high-quality assets, thereby offering transparent and economically consistent explanations of portfolio decisions.

Nevertheless, several limitations warrant careful consideration. First, the hierarchical architecture is not strictly end-to-end, as the upper- and lower-level agents are optimized in a staged manner, which may constrain full cross-level information integration. Second, although dynamic clustering enhances intra-group feature representation, the framework does not explicitly capture inter-cluster dependencies, thereby risking the omission of valuable cross-asset correlations. Third, the interpretability analysis primarily relies on SHAP, which provides post-hoc rather than real-time or causality-aware explanations, leaving open questions regarding transparent monitoring of the decision process in live trading environments. Finally, the evaluation is restricted to price-based time series from the DJIA, without the inclusion of macroeconomic, sentiment, or alternative cross-market signals, which may limit generalizability to broader financial contexts. Collectively, these issues underscore both methodological and practical dimensions in which the framework can be further advanced.

Future research will seek to address these challenges along several directions. First, more integrated end-to-end optimization paradigms will be explored, enabling upper- and lower-level agents to co-adapt through shared objectives and thereby strengthen cross-level synergy. Second, graph neural networks and correlation-aware attention mechanisms will be incorporated to explicitly model inter-cluster dependencies and improve diversification. Third, interpretability will be extended toward real-time and causality-aware frameworks, facilitating continuous monitoring of portfolio decisions and validation under counterfactual scenarios. Fourth, the framework will be enriched with multi-modal and cross-market features—including macroeconomic indicators,

textual sentiment, and alternative signals—thereby improving robustness under distributional shifts. Finally, future extensions will emphasize scalability to larger universes and higher-frequency trading environments, coupled with empirical validation under realistic constraints such as transaction costs, liquidity limitations, and execution slippage. These research avenues aim to further advance the practicality, adaptability, and theoretical depth of hierarchical deep reinforcement learning for portfolio management.

7 Declarations

The authors did not receive funding from any organization for the submitted work. The authors have no relevant financial or non-financial interests to disclose.

Xiaotian Ren determined the experimental design, wrote code, participated in conducting experiments, analyzed data, created graphics, and drafted the manuscript. Nuerxiati Abudurexiti contributes to the mathematical modeling, analytical derivations, and theoretical justification of the methodology. Zhengyong Jiang participated in data analysis. Angelos Stefanidis participated in drafting the manuscript. Hongbin Liu and Jionglong Su, as corresponding authors, jointly participated in determining the experimental design and providing technical support. All authors participated in contributing to text and the content of the manuscript, including revisions and edits. All authors approve of the content of the manuscript and agree to be held accountable for the work.

8 Availability of data and materials

The data used in this experiment are financial data, without ethical or moral issues involved. The data supporting the findings of this study are available in Yahoo Finance at <https://www.finance.yahoo.com>. These data were derived from the following resources available in the public domain: Python package yfinance.

References

- Akgül A, Baykal G, Haußmann M, et al (2025) Overcoming non-stationary dynamics with evidential proximal policy optimization. arXiv preprint arXiv:250301468 <https://doi.org/10.48550/arXiv.2503.01468>
- Alzaman C (2025) Optimizing portfolio selection through stock ranking and matching: A reinforcement learning approach. Expert Systems with Applications 269:126430. <https://doi.org/https://doi.org/10.1016/j.eswa.2025.126430>
- Apergis N, Mustafa G, Malik S (2023) The role of the covid-19 pandemic in us market volatility: Evidence from the vix index. The Quarterly Review of Economics and Finance 89:27–35
- Arrow KJ (1996) The theory of risk-bearing: small and great risks. Journal of risk and uncertainty 12(2):103–111

- Ashrafzadeh M, Taheri HM, Gharehgozlu M, et al (2023) Clustering-based return prediction model for stock pre-selection in portfolio optimization using psocnn+mvf. *Journal of King Saud University - Computer and Information Sciences* 35(9):101737. <https://doi.org/https://doi.org/10.1016/j.jksuci.2023.101737>
- Atta Mills EFE, Anyomi SK (2022) A hybrid two-stage robustness approach to portfolio construction under uncertainty. *Journal of King Saud University - Computer and Information Sciences* 34(9):7735–7750. <https://doi.org/https://doi.org/10.1016/j.jksuci.2022.06.016>
- Barro D, Consigli G, Varun V (2022) A stochastic programming model for dynamic portfolio management with financial derivatives. *Journal of Banking & Finance* <https://doi.org/10.1016/j.jbankfin.2022.106445>
- Barto AG, Mahadevan S (2003a) Recent advances in hierarchical reinforcement learning. *Discrete event dynamic systems* 13(4):341–379. <https://doi.org/10.1023/A:1025696116075>
- Barto AG, Mahadevan S (2003b) Recent advances in hierarchical reinforcement learning. *Discrete event dynamic systems* 13(4):341–379. <https://doi.org/10.1023/A:1025696116075>
- Barto AG, Mahadevan S (2003c) Recent advances in hierarchical reinforcement learning. *Discrete event dynamic systems* 13(4):341–379. <https://doi.org/10.1023/A:1025696116075>
- Bengio Y, Courville A, Vincent P (2013) Representation learning: A review and new perspectives. *IEEE transactions on pattern analysis and machine intelligence* 35(8):1798–1828. <https://doi.org/10.1109/TPAMI.2013.50>
- Bertsekas DP, et al (2011) Dynamic programming and optimal control 3rd edition, volume ii. Belmont, MA: Athena Scientific 1
- Bhattacharyya R, Hossain SA, Kar S (2014) Fuzzy cross-entropy, mean, variance, skewness models for portfolio selection. *Journal of King Saud University - Computer and Information Sciences* 26(1):79–87. <https://doi.org/https://doi.org/10.1016/j.jksuci.2013.04.001>
- Bieganowski B, Ślepaczuk R (2025) Supervised autoencoder mlp for financial time series forecasting. *Journal of Big Data* 12(1):207. <https://doi.org/10.1186/s40537-025-01267-7>
- Bisi L, Sabbioni L, Vittori E, et al (2019) Risk-averse trust region optimization for reward-volatility reduction. *arXiv preprint arXiv:191203193* <https://doi.org/10.48550/arXiv.1912.03193>

- Bodnar T, Parolya N, Schmid W (2015a) A closed-form solution of the multi-period portfolio choice problem for a quadratic utility function. *Annals of Operations Research* 229(1):121–158
- Bodnar T, Parolya N, Schmid W (2015b) On the exact solution of the multi-period portfolio choice problem for an exponential utility under return predictability. *European Journal of Operational Research* 246(2):528–542
- Borodin A, El-Yaniv R, Gogan V (2000) On the competitive theory and practice of portfolio selection. In: *LATIN 2000: Theoretical Informatics: 4th Latin American Symposium, Punta del Este, Uruguay, April 10-14, 2000 Proceedings 4*, Springer Berlin Heidelberg, pp 173–196, https://doi.org/10.1007/10719839_19
- Brandt MW, Santa-Clara P (2006) Dynamic portfolio selection by augmenting the asset space. *The journal of Finance* 61(5):2187–2217
- Bulani V, Bezbradica M, Crane M (2025) Improving portfolio management using clustering and particle swarm optimisation. *Mathematics* 13(10). <https://doi.org/10.3390/math13101623>
- Cai W, Yang F, Yao B, et al (2025) An adaptive k-means clustering algorithm based on grid and domain centroid weights for digital twins in the context of digital transformation. *Journal of Big Data* 12(1):130. <https://doi.org/10.1186/s40537-025-01180-z>
- Camanho N, Hau H, Rey H (2022) Global portfolio rebalancing and exchange rates. *The Review of Financial Studies* 35(11):5228–5274. <https://doi.org/10.1093/rfs/hhac023>
- Çanakoğlu E, Özekici S (2009) Portfolio selection in stochastic markets with exponential utility functions. *Annals of Operations Research* 166(1):281–297
- Choi C, Kim J (2024) Outperforming the tutor: Expert-infused deep reinforcement learning for dynamic portfolio selection of diverse assets. *Knowledge-Based Systems* 294:111739. <https://doi.org/https://doi.org/10.1016/j.knosys.2024.111739>
- Chou JS, Pham TBQ (2025) Leveraging ensemble learning-based stock preselection with multiobjective investment optimization for stepwise decision-supported portfolio management. *Journal of Big Data* 12(1):1–49. <https://doi.org/10.1186/s40537-025-01202-w>
- Cover TM (1991) Universal portfolios. *Mathematical finance* 1(1):1–29. <https://doi.org/10.1111/j.1467-9965.1991.tb00002.x>
- De Asis K, Hernandez-Garcia J, Holland G, et al (2018) Multi-step reinforcement learning: A unifying algorithm. *Proceedings of the AAAI conference on artificial intelligence* 32(1). <https://doi.org/10.1609/aaai.v32i1.11631>

- Driessens J, Kuiper I, Nazliben K, et al (2019) Does interest rate exposure explain the low-volatility anomaly? *Journal of Banking & Finance* 103:51–61. <https://doi.org/https://doi.org/10.2139/SSRN.2831157>
- Dulac-Arnold G, Levine N, Mankowitz DJ, et al (2021) Challenges of real-world reinforcement learning: definitions, benchmarks and analysis. *Machine Learning* 110(9):2419–2468. <https://doi.org/10.1007/s10994-021-05961-4>
- Fabozzi FJ, Markowitz HM, Gupta F (2008) Portfolio selection. *Handbook of finance* 2:3–13. <https://doi.org/10.2307/2975974>
- Fama EF, French KR (1993) Common risk factors in the returns on stocks and bonds. *Journal of Financial Economics* 33(1):3–56. [https://doi.org/https://doi.org/10.1016/0304-405X\(93\)90023-5](https://doi.org/https://doi.org/10.1016/0304-405X(93)90023-5)
- Fischer T, Krauss C (2018) Deep learning with long short-term memory networks for financial market predictions. *European Journal of Operational Research* 270(2):654–669. <https://doi.org/https://doi.org/10.1016/j.ejor.2017.11.054>
- Franke JK, Köhler G, Biedenkapp A, et al (2020) Sample-efficient automated deep reinforcement learning. *arXiv preprint arXiv:200901555* <https://doi.org/10.48550/arXiv.2009.01555>
- Gao T, Chai Y (2018) Improving stock closing price prediction using recurrent neural network and technical indicators. *Neural Computation* 30:2833–2854. https://doi.org/10.1162/neco_a_01124
- Gu F, Jiang Z, Su J (2021) Application of features and neural network to enhance the performance of deep reinforcement learning in portfolio management. In: 2021 IEEE 6th International Conference on Big Data Analytics (ICBDA), IEEE, pp 92–97, <https://doi.org/10.1109/ICBDA51983.2021.9403044>
- Gu F, Jiang Z, García-Fernández ÁF, et al (2025) Mts: A deep reinforcement learning portfolio management framework with time-awareness and short-selling. *arXiv preprint arXiv:250304143* <https://doi.org/10.48550/arXiv.2503.04143>
- Guan M, Liu XY (2022) Explainable deep reinforcement learning for portfolio management: an empirical approach. *Proceedings of the Second ACM International Conference on AI in Finance* <https://doi.org/10.1145/3490354.3494415>, URL <https://doi.org/10.1145/3490354.3494415>
- Harris RS, Ravenscraft D (1991) The role of acquisitions in foreign direct investment: Evidence from the us stock market. *The Journal of Finance* 46(3):825–844. <https://doi.org/10.1111/j.1540-6261.1991.tb03767.x>
- Helmbold DP, Schapire RE, Singer Y, et al (1998) On-line portfolio selection using multiplicative updates. *Mathematical Finance* 8(4):325–347. <https://doi.org/10.1007/s10990-008-9030-2>

- Henderson P, Islam R, Bachman P, et al (2018) Deep reinforcement learning that matters. *Proceedings of the AAAI conference on artificial intelligence* 32(1). <https://doi.org/10.1609/aaai.v32i1.11694>
- Hochreiter S, Schmidhuber J (1997) Long short-term memory. *Neural Computation* 9(8):1735–1780. https://doi.org/10.1007/978-3-642-24797-2_4
- Hong ZW, Shann TY, Su SY, et al (2018) Diversity-driven exploration strategy for deep reinforcement learning. *Advances in neural information processing systems* 31. <https://doi.org/10.48550/arXiv.1802.04564>
- Horn RA (1990) The hadamard product. In: *Proc. Symp. Appl. Math*, pp 87–169, URL https://books.google.co.jp/books?hl=zh-CN&lr=&id=KHzHCQAAQBAJ&oi=fnd&pg=PA87&ots=SF0Hr0UaXT&sig=BOV5QFqT68-pCmjQ96Dz-Cox704&redir_esc=y#v=onepage&q&f=false
- Huang Z (2024) Predicting edwards lifesciences stock prices using machine learning model. *Advances in Economics, Management and Political Sciences* <https://doi.org/10.54254/2754-1169/105/20241951>
- INSIDER (2023) Dow stock price and chart-nyse:dow-tradingview. <https://markets.businessinsider.com/stocks/dow-stock>, accessed: 2023-05-04
- Jang J, Seong N (2023) Deep reinforcement learning for stock portfolio optimization by connecting with modern portfolio theory. *Expert Systems with Applications* 218:119556. <https://doi.org/https://doi.org/10.1016/j.eswa.2023.119556>, URL <https://www.sciencedirect.com/science/article/pii/S095741742300057X>
- Jegadeesh N (1990) Evidence of predictable behavior of security returns. *The Journal of finance* 45(3):881–898. <https://doi.org/j.1540-6261.1990.tb05110.x>
- Jiang W, Liu M, Xu M, et al (2024a) New reinforcement learning based on representation transfer for portfolio management. *Knowledge-Based Systems* 293:111697. <https://doi.org/https://doi.org/10.1016/j.knosys.2024.111697>
- Jiang Y, Olmo J, Atwi M (2024b) Deep reinforcement learning for portfolio selection. *Global Finance Journal* <https://doi.org/10.1016/j.gfj.2024.101016>
- Jiang Y, Olmo J, Atwi M (2024c) Deep reinforcement learning for portfolio selection. *Global Finance Journal* <https://doi.org/10.1016/j.gfj.2024.101016>
- Jiang Z, Xu D, Liang J (2017) A deep reinforcement learning framework for the financial portfolio management problem. *arXiv preprint arXiv:170610059* <https://doi.org/10.48550/arXiv.1706.10059>

- Jiang Z, Thiayagalingam J, Su J, et al (2023) Cad: Clustering and deep reinforcement learning based multi-period portfolio management strategy. arXiv preprint arXiv:231001319 <https://doi.org/10.48550/arXiv.2310.01319>
- Jin H, Xu ZQ, Zhou XY (2008) A convex stochastic optimization problem arising from portfolio selection. Mathematical Finance 18(1):171–183. <https://doi.org/10.1111/j.1467-9965.2007.00327.x>, URL <https://doi.org/10.1111/j.1467-9965.2007.00327.x>
- Jin X, Han J (2010) K-means clustering. In: Sammut C, Webb GI (eds) Encyclopedia of Machine Learning. Springer US, Boston, MA, p 563–564, https://doi.org/10.1007/978-0-387-30164-8_425
- Kalra R, Singh T, Mishra S, et al (2024) An efficient hybrid approach for forecasting real-time stock market indices. Journal of King Saud University - Computer and Information Sciences 36(8):102180. <https://doi.org/https://doi.org/10.1016/j.jksuci.2024.102180>
- Kang M, Templeton GF, Kwak DH, et al (2024) Development of an ai framework using neural process continuous reinforcement learning to optimize highly volatile financial portfolios. Knowledge-Based Systems 300:112017. <https://doi.org/https://doi.org/10.1016/j.knosys.2024.112017>
- Keating C, Shadwick WF (2002) A universal performance measure. Journal of performance measurement 6(3):59–84. URL https://people.duke.edu/~charvey/Teaching/BA453_2004/Keating_A_universal_performance.pdf
- Kelly JL (1956) A new interpretation of information rate. the bell system technical journal 35(4):917–926. <https://doi.org/10.1002/j.1538-7305.1956.tb03809.x>
- Kim JS, Kim SH, Lee KH (2022) Portfolio management framework for autonomous stock selection and allocation. IEEE Access 10:133815–133827. <https://doi.org/10.1109/ACCESS.2022.3231889>
- Kuhn D, Luenberger DG (2010) Analysis of the rebalancing frequency in log-optimal portfolio selection. Quantitative Finance 10(2):221–234. <https://doi.org/10.1080/14697680802629400>
- Kuleshov V, Fenner N, Ermon S (2018) Accurate uncertainties for deep learning using calibrated regression. In: International conference on machine learning, PMLR, pp 2796–2804, <https://doi.org/10.48550/arXiv.1807.00263>
- Kyle AS (1985) Continuous auctions and insider trading. Econometrica: Journal of the Econometric Society pp 1315–1335. <https://doi.org/10.2307/1913210>
- Kyriazis NA, Papadamou S, Tzeremes P (2023) Are benchmark stock indices, precious metals or cryptocurrencies efficient hedges against crises? Economic Modelling 128:106502. <https://doi.org/https://doi.org/10.1016/j.econmod.2023.106502>

- LeCun Y, Bottou L, Bengio Y, et al (1998) Gradient-based learning applied to document recognition. *Proceedings of the IEEE* 86(11):2278–2324. <https://doi.org/10.1109/5.726791>
- LeCun Y, Bengio Y, Hinton G (2015) Deep learning. *nature* 521(7553):436–444. <https://doi.org/10.1038/nature14539>
- Levy A, Konidaris G, Platt R, et al (2017) Learning multi-level hierarchies with hindsight. *arXiv preprint arXiv:171200948* <https://doi.org/10.48550/arXiv.1712.00948>
- Li B, Hoi SC (2014) Online portfolio selection: A survey. *ACM Computing Surveys (CSUR)* 46(3):1–36. <https://doi.org/10.1145/2512962>
- Li B, Hoi SC, Gopalkrishnan V (2011a) Corn: Correlation-driven nonparametric learning approach for portfolio selection. *ACM Transactions on Intelligent Systems and Technology (TIST)* 2(3):1–29. <https://doi.org/10.1145/1961189.1961193>
- Li B, Hoi SC, Zhao P, et al (2011b) Confidence weighted mean reversion strategy for on-line portfolio selection. In: *Proceedings of the Fourteenth International Conference on Artificial Intelligence and Statistics, JMLR Workshop and Conference Proceedings*, pp 434–442, URL <https://proceedings.mlr.press/v15/li11b/li11b.pdf>
- Li B, Zhao P, Hoi SC, et al (2012) Pamr: Passive aggressive mean reversion strategy for portfolio selection. *Machine learning* 87:221–258. <https://doi.org/10.1007/s10994-012-5281-z>
- Li J, Zhang Y, Yang X, et al (2023) Online portfolio management via deep reinforcement learning with high-frequency data. *Information Processing & Management* 60(3):103247. <https://doi.org/https://doi.org/10.1016/j.ipm.2022.103247>, URL <https://www.sciencedirect.com/science/article/pii/S030645732200348X>
- Lillicrap TP, Hunt JJ, Pritzel A, et al (2015a) Continuous control with deep reinforcement learning. *arXiv preprint arXiv:150902971* <https://doi.org/10.48550/arXiv.1509.02971>
- Lillicrap TP, Hunt JJ, Pritzel A, et al (2015b) Continuous control with deep reinforcement learning. *arXiv preprint arXiv:150902971* <https://doi.org/10.48550/arXiv.1509.02971>
- Liu S, Chen T, Chen X, et al (2022) More convnets in the 2020s: Scaling up kernels beyond 51x51 using sparsity. *arXiv preprint arXiv:220703620* <https://doi.org/10.48550/arXiv.2207.03620>
- Liu XY, Yang H, Chen Q, et al (2020) Finrl: A deep reinforcement learning library for automated stock trading in quantitative finance. *arXiv preprint arXiv:201109607* <https://doi.org/10.48550/arXiv.2011.09607>

- Lo AW, MacKinlay AC, Zhang J (2002) Econometric models of limit-order executions. *Journal of Financial Economics* 65(1):31–71. [https://doi.org/10.1016/S0304-405X\(02\)00134-4](https://doi.org/10.1016/S0304-405X(02)00134-4)
- Lowe R, Wu YI, Tamar A, et al (2017) Multi-agent actor-critic for mixed cooperative-competitive environments. *Advances in neural information processing systems* 30. <https://doi.org/10.48550/arXiv.1706.02275>
- Lundberg SM, Lee SI (2017) A unified approach to interpreting model predictions. In: *Proceedings of the 31st International Conference on Neural Information Processing Systems*. Curran Associates Inc., Red Hook, NY, USA, NIPS’17, p 4768–4777, <https://doi.org/10.48550/arXiv.1705.07874>
- Ma Y, Mao R, Lin Q, et al (2024) Quantitative stock portfolio optimization by multi-task learning risk and return. *Information Fusion* 104:102165. <https://doi.org/10.1016/j.inffus.2023.102165>
- Micikevicius P, Narang S, Alben J, et al (2017) Mixed precision training. *arXiv preprint arXiv:171003740* <https://doi.org/10.48550/arXiv.1710.03740>
- Mitra Thakur GS, Bhattacharyya R, Sarkar (Mondal) S (2018) Stock portfolio selection using dempster–shafer evidence theory. *Journal of King Saud University - Computer and Information Sciences* 30(2):223–235. <https://doi.org/https://doi.org/10.1016/j.jksuci.2016.07.001>
- Mnih V, Kavukcuoglu K, Silver D, et al (2015) Human-level control through deep reinforcement learning. *Nature* 518(7540):529–533. <https://doi.org/10.1038/nature14236>
- Moody J, Saffell M (2001) Learning to trade via direct reinforcement. *IEEE transactions on neural Networks* 12(4):875–889. <https://doi.org/10.1109/72.935097>
- Moskowitz TJ, Ooi YH, Pedersen LH (2012) Time series momentum. *Journal of Financial Economics* 104(2):228–250. <https://doi.org/https://doi.org/10.1016/j.jfineco.2011.11.003>, special Issue on Investor Sentiment
- Namitha K, Santhosh Kumar G (2020) Learning in the presence of concept recurrence in data stream clustering. *Journal of Big Data* 7(1):75. <https://doi.org/10.1186/s40537-020-00354-1>
- Oyewola DO, Akinwunmi SA, Omotehinwa TO (2024) Deep lstm and lstm-attention q-learning based reinforcement learning in oil and gas sector prediction. *Knowledge-Based Systems* 284:111290. <https://doi.org/https://doi.org/10.1016/j.knosys.2023.111290>
- Patilea V, Raïssi H (2014) Testing second-order dynamics for autoregressive processes in presence of time-varying variance. *Journal of the American Statistical Association*

109(507):1099–1111. <https://doi.org/10.1080/01621459.2014.884504>

Peng J, Chao K, Chen G, et al (2024a) An online portfolio selection algorithm with dynamic coresnet construction. In: International Conference on Knowledge Science, Engineering and Management, Springer, pp 27–37, https://doi.org/10.1007/978-981-97-5489-2_3

Peng J, Chao K, Chen G, et al (2024b) An online portfolio selection algorithm with dynamic coresnet construction. In: Knowledge Science, Engineering and Management. Springer Nature Singapore, Singapore, pp 27–37

Peng Q, An S, Nie S, et al (2025) Collar: combating low-rank temporal latent representation for high-dimensional multivariate time series prediction using dynamic koopman regularization. *Journal of Big Data* 12(1):258. <https://doi.org/10.1186/s40537-025-01299-z>

Polamuri SR, Srinivas DK, Krishna Mohan DA (2022) Multi-model generative adversarial network hybrid prediction algorithm (mmgan-hpa) for stock market prices prediction. *Journal of King Saud University - Computer and Information Sciences* 34(9):7433–7444. <https://doi.org/https://doi.org/10.1016/j.jksuci.2021.07.001>

Poli R, Kennedy J, Blackwell T (2007) Particle swarm optimization: An overview. *Swarm intelligence* 1(1):33–57. <https://doi.org/10.1007/s11721-007-0002-0>

Pratt JW (1978) Risk aversion in the small and in the large. In: Uncertainty in economics. Elsevier, p 59–79

Qin Y, Gu F, Su J (2022) A novel deep reinforcement learning strategy for portfolio management. In: 2022 7th International Conference on Big Data Analytics (ICBDA), IEEE, pp 366–372, <https://doi.org/10.1109/ICBDA55095.2022.9760348>

Rásonyi M, Sayit H (2025) Exponential utility maximization in small/large financial markets. *Modern Stochastics: Theory and Applications* 12(2):225–250

Ren X, Jiang Z, Su J (2021) The use of features to enhance the capability of deep reinforcement learning for investment portfolio management. In: 2021 IEEE 6th International Conference on Big Data Analytics (ICBDA), IEEE, pp 44–50, <https://doi.org/10.1109/ICBDA51983.2021.9403019>

Ren X, Sun R, Jiang Z, et al (2025) Time series is not enough: Financial transformer reinforcement learning for portfolio management. *Neurocomputing* p 130451. <https://doi.org/10.1016/j.neucom.2025.130451>

Rollinger TN, Hoffman ST (2013) Sortino: a ‘sharper’ratio. Chicago, Illinois: Red Rock Capital URL <https://ea.kitgain.com/content/uploadfile/202102/9e631613532179.pdf>

SAID SE, DICKEY DA (1984) Testing for unit roots in autoregressive-moving average models of unknown order. *Biometrika* 71(3):599–607. <https://doi.org/10.1093/biomet/71.3.599>

Sharpe WF (1964) Capital asset prices: A theory of market equilibrium under conditions of risk. *The journal of finance* 19(3):425–442. <https://doi.org/10.1111/j.1540-6261.1964.tb02865.x>

Sharpe WF (1998) The sharpe ratio. *Streetwise—the Best of the Journal of Portfolio Management* 3:169–185. <https://doi.org/10.1515/9781400829408-022>

Shen J, Shafiq MO (2020) Short-term stock market price trend prediction using a comprehensive deep learning system. *Journal of big Data* 7(1):66. <https://doi.org/10.1186/s40537-020-00333-6>

Shi W, Song S, Wu H, et al (2019) Regularized anderson acceleration for off-policy deep reinforcement learning. *Advances in Neural Information Processing Systems* 32. <https://doi.org/10.48550/arXiv.1909.03245>

Shu Y, Yu C, Mulvey JM (2024) Downside risk reduction using regime-switching signals: a statistical jump model approach. *Journal of Asset Management* 25(5):493–507. <https://doi.org/10.1057/s41260-024-00376-x>

Silver D, Lever G, Heess N, et al (2014) Deterministic policy gradient algorithms. In: Xing EP, Jebara T (eds) *Proceedings of the 31st International Conference on Machine Learning, Proceedings of Machine Learning Research*, vol 32. PMLR, Beijing, China, pp 387–395, URL <https://proceedings.mlr.press/v32/silver14.html>

Sun R, Jiang Z, Su J (2021) A deep residual shrinkage neural network-based deep reinforcement learning strategy in financial portfolio management. In: 2021 IEEE 6th International Conference on Big Data Analytics (ICBDA), IEEE, pp 76–86, <https://doi.org/10.1109/ICBDA51983.2021.9403210>

Sun R, Stefanidis A, Jiang Z, et al (2024) Combining transformer based deep reinforcement learning with black-litterman model for portfolio optimization. *Neural Computing and Applications* 36(32):20111–20146. <https://doi.org/10.1007/s00521-024-09805-9>

Sun R, Xi Y, Stefanidis A, et al (2025) A novel multi-agent dynamic portfolio optimization learning system based on hierarchical deep reinforcement learning. *Complex & Intelligent Systems* 11(7):311. <https://doi.org/10.1007/s40747-025-01884-y>

Sun S, Qin M, Zhang W, et al (2023) Trademaster: A holistic quantitative trading platform empowered by reinforcement learning. *Advances in Neural Information Processing Systems* 36:59047–59061. URL <https://openreview.net/forum?id=17Ggnzaws5>

- Sutton R, Barto A (1998) Reinforcement learning: An introduction. *IEEE Transactions on Neural Networks* 9(5):1054–1054. <https://doi.org/10.1109/TNN.1998.712192>
- Trosten DJ, Jenssen R, Kampffmeyer MC (2021) Reducing objective function mismatch in deep clustering with the unsupervised companion objective. *Proceedings of the Northern Lights Deep Learning Workshop* 2:2419–2468. <https://doi.org/10.7557/18.5709>
- Trucíos C (2025) Hierarchical risk clustering versus traditional risk-based portfolios: an empirical out-of-sample comparison. Available at SSRN 5247627 <https://doi.org/10.2139/ssrn.5247627>
- Ullah S, Khan S, Hashmi NI, et al (2023) Covid-19 pandemic and financial market volatility: A quantile regression approach. *Heliyon* 9(10). <https://doi.org/https://doi.org/10.1016/j.heliyon.2023.e21131>
- Ulm G, Smith S, Nilsson A, et al (2020) S-raster: contraction clustering for evolving data streams. *Journal of Big Data* 7(1):62. <https://doi.org/10.1186/s40537-020-00336-3>
- Vaswani A, Shazeer N, Parmar N, et al (2017) Attention is all you need. *Advances in neural information processing systems* 30. <https://doi.org/10.48550/arXiv.1706.03762>
- Walauskis MA, Khoshgoftaar TM (2025) A novel approach to automating unsupervised estimation of class distribution. *Journal of Big Data* 12(1):1–29. <https://doi.org/10.1186/s40537-025-01231-5>
- Wang S, Gupta R, Zhang YJ (2021) Bear, bull, sidewalk, and crash: the evolution of the us stock market using over a century of daily data. *Finance Research Letters* 43:101998. <https://doi.org/https://doi.org/10.1016/J.FRL.2021.101998>
- Wang Y, Aste T (2023) Dynamic portfolio optimization with inverse covariance clustering. *Expert Systems with Applications* 213:118739. <https://doi.org/10.1016/j.eswa.2022.118739>
- Wei S, hua Gao X, Zhang Y, et al (2021) An improved stochastic model predictive control operation strategy of integrated energy system based on a single-layer multi-timescale framework. *Energy* 235:121320. <https://doi.org/10.1016/J.ENERGY.2021.121320>
- Xiao H, Zhou Z, Ren T, et al (2020) Time-consistent strategies for multi-period mean-variance portfolio optimization with the serially correlated returns. *Communications in Statistics-Theory and Methods* 49(12):2831–2868. <https://doi.org/10.1080/03610926.2019.1636999>

- Xiong H, Yang G, Wang Z (2022) Factor portfolio and target volatility management: An analysis of portfolio performance in the us and china. *International Review of Economics & Finance* 79:493–517. <https://doi.org/https://doi.org/10.1016/j.iref.2022.02.011>
- Xu Y, Song Y, Pi D, et al (2023) A reinforcement learning-based multi-objective optimization in an interval and dynamic environment. *Knowledge-Based Systems* 280:111019. <https://doi.org/https://doi.org/10.1016/j.knosys.2023.111019>
- Yan R, Jin J, Han K (2024) Reinforcement learning for deep portfolio optimization. *Electronic Research Archive* 32(9). <https://doi.org/10.3934/era.2024239>
- Yang B, Liang T, Xiong J, et al (2023) Deep reinforcement learning based on transformer and u-net framework for stock trading. *Knowledge-Based Systems* 262:110211. <https://doi.org/https://doi.org/10.1016/j.knosys.2022.110211>
- Yang H, Liu XY, Zhong S, et al (2020a) Deep reinforcement learning for automated stock trading: An ensemble strategy. In: Proceedings of the first ACM international conference on AI in finance, pp 1–8, <https://doi.org/10.1145/3383455.3422540>
- Yang H, Liu XY, Zhong S, et al (2020b) Deep reinforcement learning for automated stock trading: An ensemble strategy. In: Proceedings of the first ACM international conference on AI in finance, pp 1–8, <https://doi.org/10.1145/3383455.3422540>
- Yang S (2023) Deep reinforcement learning for portfolio management. *Knowledge-Based Systems* 278:110905. <https://doi.org/https://doi.org/10.1016/j.knosys.2023.110905>
- Zhang Y, Zhao P, Wu Q, et al (2020) Cost-sensitive portfolio selection via deep reinforcement learning. *IEEE Transactions on Knowledge and Data Engineering* 34(1):236–248. <https://doi.org/10.1109/TKDE.2020.2979700>
- Zhao T, Ma X, Li X, et al (2023) Asset correlation based deep reinforcement learning for the portfolio selection. *Expert Systems with Applications* 221:119707. <https://doi.org/https://doi.org/10.1016/j.eswa.2023.119707>, URL <https://www.sciencedirect.com/science/article/pii/S0957417423002087>
- Zhao Z, Welsch RE (2024a) Hierarchical reinforced trader (hrt): A bi-level approach for optimizing stock selection and execution. *arXiv preprint arXiv:241014927*
- Zhao Z, Welsch RE (2024b) Hierarchical reinforced trader (hrt): A bi-level approach for optimizing stock selection and execution. *arXiv preprint arXiv:241014927* <https://doi.org/10.48550/arXiv.2410.14927>
- Zheng S, Song Y, Leung T, et al (2016) Improving the robustness of deep neural networks via stability training. In: 2016 IEEE Conference on Computer Vision and Pattern Recognition (CVPR), IEEE, pp 4480–4488, <https://doi.org/10.1109/CVPR.2016.75>

CVPR.2016.485

Zouaghia Z, Kodia Z, Ben said L (2025) A novel approach for dynamic portfolio management integrating k-means clustering, mean-variance optimization, and reinforcement learning; Z. zouaghia et al. Knowledge and Information Systems pp 1–73.
<https://doi.org/10.1007/s10115-025-02475-6>